Helicopter Blade Dynamic Loads Measured During Performance Testing of Two Scaled Rotors

John D. Berry

NASA

US ARMY
AVIATION
SYSTEMS COMMAND
AVIATION R&T ACTIVITY

Helicopter Blade Dynamic Loads Measured During Performance Testing of Two Scaled Rotors

John D. Berry

Aerostructures Directorate
USAARTA-AVSCOM
Langley Research Center
Hampton, Virginia

CONTENTS

SUMMARY

A test to determine the performance differences between the 27-percent-scale models of two rotors for the U.S. Army AH-64 helicopter was conducted in the Langley 14- by 22-Foot Subsonic Tunnel. One rotor, referred to as the "baseline rotor," simulated the geometry and dynamic characteristics of the production baseline rotor, and the other rotor, referred to as the "advanced rotor," was designed to have improved hover performance. During the performance test, the dynamic pitch-link forces and blade bending and torsion moments were also measured. Dynamic data from the forward flight investigation have been reduced and are presented herein. The advanced blade set was designed to have dynamic characteristics similar to those of the baseline rotor so that test conditions would not be limited by potential rotor instability and blade resonances and so that the measured performance increments could be considered to be due purely to aerodynamic causes. Data show consistent trends with advance ratio for both blade sets with generally higher oscillatory loads occurring for the advanced blade set when compared with the baseline blade set.

INTRODUCTION

A test to determine the performance differences between two helicopter 27-percent-scale model rotors for the U.S. Army AH-64 helicopter was conducted in the Langley 14- by 22-Foot Subsonic Tunnel (formerly known as the 4- by 7-Meter Tunnel). One set of blades, which was scaled both in geometry and in dynamic characteristics to represent the current production blade set (ref. 1), was designated as the "baseline configuration," and a second set of blades, which was designed to improve the static performance characteristics of the helicopter, was designated as an "advanced configuration" (ref. 2). Both blade sets were designed to have the same basic dynamic characteristics. The test was conducted in hover and over a range of forward speeds for an advance ratio from 0.10 to 0.30 with values of full-scale thrust (lift) up to 20 500 lb (1.4g - where 1g $\approx$ 32.17 ft/sec^2). Although the primary purpose of the wind-tunnel tests was to evaluate performance differences of the two rotors, the rotor blades and pitch link were instrumented to measure blade loading as well. This report presents the blade load data obtained during the test so that a correlation may be made with analytical predictions.

NOTATION

The measurements used in this report were made in U.S. Customary Units. All measurements were made in the rotating system along the elastic axis of the blade (fig. 1).

Symbols and Abbreviations

A_1 blade lateral cyclic pitch, deg

B_1 blade longitudinal cyclic pitch, deg

C_T	rotor thrust coefficient, $T/\rho\pi R^2(\Omega R)^2$
c	local blade chord, in.
c.g.	center of gravity
P-P	peak-to-peak value for signal
pho	pitch horn offset, 2.63 in.
R	rotor radius, 6.48 ft
r	local radius
1/rev	one per revolution
T	thrust of rotor, lb
x	distance from leading edge, in.
α	fuselage angle of attack (shaft offset 5°), deg
θ	blade collective pitch at 0.75R, deg
μ	advance ratio (Mu used in computer printouts)
ρ	density of tunnel air, slugs/ft^3
Ω	rotor rotational speed, 112 rad/sec

Measured Quantities

beam	out-of-plane bending-moment measurement, in-lb
chord	in-plane bending-moment measurement, in-lb
P-L	force in pitch-change link, lb
torsion	torsion about elastic axis of blade, in-lb

Nominal Values

C_T 0.0064

Thrust, lb 1070

MODEL AND APPARATUS

This test was conducted in the Langley 14- by 22-Foot Subsonic Tunnel (ref. 3) using a 27-percent-scale model of the U.S. Army AH-64 helicopter mounted on the Army/NASA General Rotor Model System (GRMS) described in reference 4. (See fig. 2.)

A rotor hub that used a "strap-pack" tension relief system scaled closely from the U.S. Army AH-64 helicopter was used in this investigation (ref. 1). Lead-lag (in-plane) freedom was allowed about a pivot near the end of the pitch cuff and was damped in motion by dual elastomeric dampers. Flapping freedom and feathering freedom were allowed by a sliding spherical bearing. Leading pitch links with no pitch-flap coupling were used.

The baseline and advanced blade sets shown in figure 3 were constructed of composite materials. The baseline blades were built to scale the production AH-64 blades in both geometry and dynamic characteristics. The mass and stiffness of the blades were distributed according to Mach-scaling laws to match the scaled frequencies and fundamental modes of the full-scale blades. A comparison of weight distributions for an exactly scaled AH-64 blade and the baseline model blade design is shown in figure 4. The advanced blade set was designed with altered planform, airfoil sections, and twist distribution for improved hovering performance without degrading forward flight performance. The mass and stiffness distributions of the advanced blades were selected to provide frequencies similar to those of the baseline blades and to avoid potential rotor system instabilities (fig. 5). Such an instability was predicted for the baseline rotor system, as mounted on the GRMS, and the damping within the GRMS was increased to reduce that potential problem (ref. 1).

To illustrate the ability to match blade properties, table I(a) compares the calculated principal structural properties of the constant chord sections of the two blades. The distributions of sectional properties with radius were similarly matched, as shown in figures 4 and 5, with two exceptions: (1) in the tip region of the advanced blade, there was insufficient volume for good matching of these properties; and (2) because of a larger section area in the advanced blade constant chord region, the sectional inertia was larger. Table I(b) lists the natural frequencies for the two rotor blade sets. The experimental values were obtained by shake testing each of the blades suspended from the model rotor hub. The computed values were obtained from reference 2. The advanced blade design used airfoils developed by the U.S. Army Aerostructures Directorate at the NASA Langley Research Center (ref. 5). The twist of both blade sets was distributed linearly from the root to the tip. The twist of the baseline blades was -9°, and the advanced blades were twisted by -12°.

One blade of each rotor was instrumented for the measurement of dynamic loads. The loads measured were pitch-link force, root and tip torsion, three stations of in-plane (chordwise) bending, and five stations of out-of-plane (beamwise) bending. Because of blade constraints, the radial locations for the instrumented stations were different for the two rotors, and they are listed in table II. A zero-azimuth reference position was signaled by a one-per-revolution index pulse (1/rev) from the model when the blade with the instrumentation was directly over the helicopter tail.

Selected blade loads were monitored constantly during the test to ensure that the stress limits were not exceeded. During selected data points the loads were recorded on a frequency-modulated wideband tape recorder. The tape recording system was set for a frequency response of approximately 20 kHz. A time code sequence was recorded along with the data to allow indexing of the tape and the 1/rev pulse signal for azimuth correlation.

DATA REDUCTION

The recorded data were interpreted using a multichannel analog-to-digital converter that converted up to 10 channels of analog data simultaneously into 10 significant bits of digital data for each channel at 2000 samples per second per channel. During the digitizing process, conversion of the raw data into engineering units was accomplished by using prerecorded calibration signals that were obtained for zero loading on the blade and for a known load condition on the blade. The signals for the torsion gauges were divided by the pitch-horn-offset (pho) distance to obtain equivalent pitch-link forces for comparison with the measured pitch-link forces. Conversion of the 1/rev pulse signal synchronously with the loads data allowed for a time-series analysis of the data.

The mean time history was obtained by evaluating the data in 5° increments around the azimuth. Since more than one data sample was available for each 5° increment, a linear fit was used to determine the value of the loads at the center of the specified increment based on its distance from the reference pulse. The resulting time history represents the average over a minimum of 143 revolutions. The peak-to-peak (P-P) value for the signal is obtained from the difference between the maximum and minimum values of the averaged time history.

Data for approximately four revolutions were stored into buffers for spectral conversion by a fast Fourier transform (FFT) algorithm. A Hanning window was applied to the transformed data to improve the spectral estimates since the periodic data were not conditionally sampled. Multiple conversions were made and then block averaged for spectral accuracy (ref. 6). Thirty-two or more blocks were used for each of these spectral estimates. To obtain an estimate of the value at even harmonics (1/rev, 2/rev, etc.), a cubic spline was fitted to the averaged spectra. Even though this method produced spectral lines that were not at integer harmonics of the rotational rate, this approximation of the signal at the significant harmonic values was used. The significant harmonic quantities for each signal (the first through the fifth harmonic) from the analyzed data are presented.

PRESENTATION OF RESULTS

The investigation resulted in the measurement of the dynamic forces and moments on two sets of rotor blades. The force and moment dynamic characteristics are plotted as a function of rotor forward speed (as expressed by advance ratio or tip speed ratio). A method of normalizing the test condition was therefore required in order to account for minor variations in test conditions other than rotor forward speed such as thrust, tip speed, and density.

Because the dynamic loads are influenced by the aerodynamics of the test condition, a method of normalizing the data based on these aerodynamic parameters was needed. The rotor blade aerodynamics can be related to a local dynamic pressure acting on the blade. To normalize the loads, the actual local dynamic pressure is corrected to a "normal" local dynamic pressure. Since the loads are presented as functions of advance ratio and radial position whereas the dynamic analysis is independent of azimuth, the normalization needed only to account for variations in density and rotational speed. Beam and chord moments presented will also be normalized by rotor thrust. The procedure used to normalize the data from the present investigation is described in the following discussion.

4

The recorded mean values of thrust and C_T were used to minimize errors due to variations in density, tip speed, and rotor thrust at different data recording points. For example:

$$\text{Beam normalized} = \text{Beam} \times \frac{C_T}{T^2} \left(\frac{T^2}{C_T} \right)_{\text{nominal}}$$

$$\text{Chord normalized} = \text{Chord} \times \frac{C_T}{T^2} \left(\frac{T^2}{C_T} \right)_{\text{nominal}}$$

This procedure was applied only to the chord and beam moments. Torsional moments have been divided by the pitch horn offset (pho) to produce equivalent pitching forces in all data presented. When observing the data presented, note that the radial station for measurement of the same signal is different for the two rotors. The actual locations at which the measurements were made are shown in table II.

Results of the data reduction are presented in figures 6 to 11 as shown in table III. Variation of baseline blade loads with advance ratio are presented in figures 6 to 8, and the data for the advanced blade load parameters are shown in figures 9 to 11.

Table IV presents the steady-state test conditions during the acquisition of the dynamic data presented here. Angles of attack and propulsive-force values were chosen to match nominal values obtained from flight testing (ref. 7) at the specified thrust. Tables V and VI present listings of the data used to prepare figures 6 to 11. The appendix presents a discussion of the additional analysis associated with the mean load data.

DISCUSSION

The data presented were acquired during a performance investigation of dynamically scaled powered rotors on a scaled helicopter model. The performance results are presented in reference 8. Blade and link dynamic data are presented here for use in correlating analytical tools for blade load prediction.

The primary objective during the structural design of these blades was to attain dynamic compatibility with the rotor test system. This compatibility was necessary because of the small factors of safety involved in rotor model testing. The secondary objective was to model the baseline rotor dynamic properties accurately. The structure of the advanced blade was designed to attain, as closely as possible, a predicted dynamic similarity to the baseline blade. Exact similarity was precluded, however, by the significantly larger sectional inertia caused by bending stiffness matching and by the severe volumetric restriction in the thin tip region of the advanced design.

The mean data obtained from the blade gauges used in this wind-tunnel investigation have been found to contain a component due to a spanwise load along the blade due to rotational acceleration; the appendix examines this component of load signal. The gauge sensitivity to axial strain was unexpected because the full-bridge bending and torsion gauge installed on the blades is chosen specifically to minimize

sensitivity to uniform strains. Because the blades are made entirely of composite materials, however, they have anisotropic deflection properties. The magnitude of this anisotropy, although not known quantitatively, has been observed in the sensitivity response of the full-bridge bending and torsion gauge to changes in elongational strain. This characteristic may affect the reduction and use of gauge data from practically all composite blades.

Unexpectedly high levels of the monitored dynamic signals were experienced for both rotors during testing, and these high dynamic loads imposed limits on some test conditions. The dynamic characteristics observed for the advanced design may have an impact on the final design of a full-scale blade with the specific geometry and structure used in this test. Two general observations from the data presented are that (1) the baseline rotor experienced, on the whole, lower levels of blade loads than the advanced rotor for the same flight conditions, and (2) the principal harmonic contents of the signals show definite trends with advance ratio. Direct comparisons of the data from these two rotors must, however, be restricted to simple observations because of the nature of the blade structural design and the design of the experiment in which these measurements were made; that is, the advanced blade was not designed to minimize dynamic blade loading.

The experiment in which these measurements were made was designed to determine the steady-state performance characteristics of the advanced blade design when compared with those of the baseline blade; the measurement of the dynamic signals was incidental to the major thrust of the test. The influence of blade dynamic characteristics on vehicle static performance has not yet been well-defined by flight or model testing. Since the investigation was designed only for steady-state performance measurements, no parameter variation was attempted to affect dynamics during this test.

CONCLUDING REMARKS

A test to determine the performance differences between the 27-percent-scale models of two rotors for the U.S. Army AH-64 helicopter was conducted in the Langley 14- by 22-Foot Subsonic Tunnel. One rotor, referred to as the "baseline rotor," simulated the geometry and dynamic characteristics of the production baseline rotor, and the other rotor, referred to as the "advanced rotor," was designed to have improved hover performance. Both rotors showed consistent trends in the principal harmonic content of dynamic blade loads as a function of advance ratio. Differences in radial location of measurements between the two blade sets should be noted carefully when attempting any detailed comparison. The oscillatory data presented are a good representation of the observed real-time characteristics of the rotors. The advanced blade set generally experienced higher dynamic loads than the baseline blade set; however, the advanced blades were not designed to reduce those loads.

A further observation to be made is that the anisotropic material properties of composite rotor blades must be considered when using strain gauges to determine blade loads. The sensitivity of installed gauges to the rotationally induced axial loads should be investigated for rotor blades where the load information is a critical element of the design or evaluation process.

NASA Langley Research Center
Hampton, VA 23665-5225
April 17, 1987

REFERENCES

1. Straub, F. K.; Johnston, R. A.; Head, R. E.; and Kelley, H. L.: Design and Development of a Dynamically Scaled Model AH-64 Main Rotor. Vertica, vol. 9, no. 2, 1985, pp. 165-180.

2. Bingham, Gene J.: The Aerodynamic Influences of Rotor Blade Airfoils, Twist, Taper and Solidity on Hover and Forward Flight Performance. Proceedings of the 37th Annual Forum, American Helicopter Soc., May 1981, pp. 37-50.

3. Applin, Zachary T.: Flow Improvements in the Circuit of the Langley 4- by 7-Meter Tunnel. NASA TM-85662, 1983.

4. Wilson, John C.: A General Rotor Model System for Wind-Tunnel Investigations. J. Aircr., vol. 14, no. 7, July 1977, pp. 639-643.

5. Bingham, Gene J.; and Noonan, Kevin W.: Two-Dimensional Aerodynamic Characteristics of Three Rotorcraft Airfoils at Mach Numbers From 0.35 to 0.90. NASA TP-2000, AVRADCOM TR 82-B-2, 1982.

6. Bendat, Julius S.; and Piersol, Allan G.: Engineering Applications of Correlation and Spectral Analysis. John Wiley & Sons, Inc., c.1980.

7. Bender, Gary L.; Higgins, Larry B.; Savage, Richard; Ottomeyer, John D.; Picasso, Bartholomew D., III; and Morris, Patrick M.: Airworthiness and Flight Characteristics Test. Part 1 - YAH-64 Advanced Attack Helicopter. USAAEFA No. 80-17-1, U.S. Army, Sept. 1981. (Available from DTIC as AD A118 490.)

8. Kelley, H. L.; and Wilson, J. C.: Aerodynamic Performance of a 27-Percent-Scale AH-64 Wind-Tunnel Model With Baseline/Advanced Rotor Blades. Proceedings of the 41st Annual Forum, American Helicopter Soc., May 1985, pp. 491-499.

TABLE I.- BLADE CHARACTERISTICS

(a) Calculated structural characteristics of constant chord blade section

Characteristic	Baseline blade	Advanced blade
c, in.	5.67	7.00
x/c elastic axis, percent	20	26
Bending stiffness in plane, lb-in^2	4.44×10^6	6.30×10^6
Bending stiffness out of plane, lb-in^2	106.9×10^3	124.2×10^3
Torsional stiffness, lb-in^2	124.5×10^3	116.5×10^3
Weight distribution, lb/in.	0.0368	0.0373
Sectional inertia, lb-in.	0.0684	0.1534
x/c of c.g., percent of local chord length	26.5	26.2

(b) Rotor blade natural frequencies

Mode	Experimental frequency, Hz (a)		(Computed frequency)/Ω (b)	
	Baseline	Advanced	Baseline	Advanced
Rigid body lag			0.51	0.60
Rigid body flap			1.04	1.05
First flap	14.3	18.3	2.75	2.78
Second flap	49.5	60.3	4.62	5.39
First chord	96.3	99.3	6.32	6.88
First torsion	130.0	120.0	5.27	4.03

[a]Experimental values are measured with blade suspended from hub.
[b]Computed values are taken from reference 1.

TABLE II.- RADIAL LOCATIONS FOR BLADE INSTRUMENTATION

| Measurements (a) | Fraction of blade radius, r/R, for - | |
	Baseline blade	Advanced blade
Beam 1	0.19	0.18
Chord 1	0.19	0.18
Torsion 1	0.36	0.28
Beam 2	0.36	0.28
Chord 2	0.36	0.28
Torsion 2	0.93	0.77
Beam 3	0.60	0.47
Chord 3	0.60	0.47
Beam 4	0.77	0.60
Beam 5	0.93	0.77

[a]Numbers indicate radial order of occurrence.

TABLE III.- LISTING OF DATA FIGURES

| Blade | Figure | | Data shown for - |
	Description	Number	
Baseline	Chord bending moment	6(a) (b) (c) (d) (e) (f)	1/rev 2/rev 3/rev 4/rev 5/rev 1/2 P-P
	Beam bending moment	7(a) (b) (c) (d) (e) (f)	1/rev 2/rev 3/rev 4/rev 5/rev 1/2 P-P
	Equivalent P-L forces	8(a) (b) (c) (d) (e) (f)	1/rev 2/rev 3/rev 4/rev 5/rev 1/2 P-P
Advanced	Chord bending moment	9(a) (b) (c) (d) (e) (f)	1/rev 2/rev 3/rev 4/rev 5/rev 1/2 P-P
	Beam bending moment	10(a) (b) (c) (d) (e) (f)	1/rev 2/rev 3/rev 4/rev 5/rev 1/2 P-P
	Equivalent P-L forces	11(a) (b) (c) (d) (e) (f)	1/rev 2/rev 3/rev 4/rev 5/rev 1/2 P-P

TABLE IV.- TEST CONDITIONS FOR DYNAMIC MEASUREMENTS

(a) Advanced blade

μ	α, deg	T, lb	c_T	θ, deg	B_1, deg	A_1, deg
0.100	-0.53	1045.4	0.00645	5.05	2.18	-2.94
.151	-1.48	1055.2	.00647	4.56	2.94	-2.28
.200	-3.03	1051.2	.00654	5.25	3.95	-1.83
.252	-4.33	1151.9	.00703	7.25	5.62	-1.75
.299	-5.66	1178.7	.00736	9.49	7.48	-1.77

(b) Baseline blade

μ	α, deg	T, lb	c_T	θ, deg	B_1, deg	A_1, deg
0.100	-0.58	1276.9	0.00774	7.39	2.35	-2.51
.149	-1.57	1052.7	.00653	5.46	2.91	-1.72
.206	-3.04	1045.3	.00655	5.98	3.96	-1.23
.250	-4.68	1063.9	.00676	7.65	5.87	-.95
.300	-5.94	1052.8	.00662	8.90	7.22	-.90

TABLE V.- SPECTRAL CONTENT OF MEASUREMENTS ON BASELINE BLADE

[Chord and beam are measured in inch-pounds; torsion (Tors) and P-L are presented in pounds]

Mu	1/rev	2/rev	3/rev	4/rev	5/rev	1/2 P-P
Chord 1	.19					
.9993E-01	107.4	28.92	60.90	16.24	37.11	248.3
.1495	148.7	28.00	40.51	24.21	26.65	292.4
.2063	168.7	30.67	28.49	24.53	21.28	317.0
.2502	177.4	29.91	37.44	35.41	23.53	329.3
.2998	203.4	26.96	62.34	51.00	27.02	358.0
Chord 2	.36					
.9993E-01	87.21	34.52	76.56	28.51	53.48	280.1
.1495	110.4	30.48	44.20	32.57	32.91	283.1
.2063	139.3	32.12	32.15	33.14	22.80	336.5
.2502	153.6	32.92	45.29	48.57	24.64	354.3
.2998	177.8	33.30	69.53	66.79	33.48	346.3
Chord 3	.60					
.9993E-01	46.57	37.10	46.87	28.77	32.24	220.2
.1495	56.87	35.35	30.07	31.49	19.13	215.3
.2063	79.87	37.29	26.54	28.30	14.04	258.0
.2502	94.12	37.38	35.55	37.61	15.38	276.8
.2998	110.5	29.82	46.19	55.84	27.50	233.3
Beam 1	.19					
.9993E-01	5.615	4.609	26.93	16.07	25.46	93.25
.1495	4.296	5.593	23.51	12.73	22.56	82.53
.2063	3.318	12.09	17.29	7.969	10.77	60.81
.2502	10.81	21.13	23.72	6.685	9.069	80.61
.2998	14.61	33.60	31.27	7.372	5.793	99.18
Beam 2	.36					
.9993E-01	.4968E-01	.4007E-01	.1215	.5153E-01	.3336	13.52
.1495	.1253	.1360	.4631	.2046	.1087	2.413
.2063	.1227	.1232	.4403	.2171	1.025	2.455
.2502	.1022	.1217	.4445	.2085	.9658	2.273
.2998	.8806E-01	.1077	.3406	.1589	.8082	2.239
Beam 3	.60					
.9993E-01	25.42	15.34	24.93	6.946	16.07	78.67
.1495	24.35	24.08	22.36	4.477	11.71	79.78
.2063	35.59	28.19	19.63	4.211	4.573	87.58
.2502	42.68	28.77	24.12	4.003	3.211	96.97
.2998	54.52	33.32	24.28	9.197	3.967	111.7
Beam 4	.77					
.9993E-01	27.04	36.24	22.77	23.38	23.75	120.4
.1495	17.20	35.10	20.82	9.668	16.19	107.4
.2063	22.48	36.23	22.82	9.753	10.33	103.8
.2502	26.96	35.30	21.89	10.94	6.037	97.66
.2998	34.80	36.48	15.36	9.460	4.178	85.61
Beam 5	.93					
.9993E-01	9.577	14.59	5.537	10.80	7.867	46.26
.1495	7.927	9.867	3.932	6.727	5.183	43.00
.2063	9.490	7.883	4.294	4.078	3.471	38.41
.2502	12.15	7.427	4.305	3.119	1.902	32.28
.2998	14.99	8.119	2.943	1.851	1.825	30.06

TABLE V.- Concluded

Mu	1/rev	2/rev	3/rev	4/rev	5/rev	1/2 P-P
P-L	.05					
.9993E-01	9.360	5.266	.9370	5.133	3.859	26.66
.1495	8.148	2.293	.5641	1.584	1.863	18.08
.2063	9.103	2.919	1.025	1.195	1.411	19.03
.2502	11.08	3.798	2.038	1.657	1.375	19.96
.2998	12.10	5.902	4.059	.9778	2.817	25.68
Tors 1/pho	.19					
.9993E-01	7.161	2.966	1.313	2.748	2.862	16.71
.1495	6.126	1.776	.6925	.5848	1.469	11.93
.2063	7.104	2.198	.6478	.5689	1.274	12.32
.2502	8.635	3.036	1.181	1.111	.8770	14.77
.2998	10.34	5.171	2.403	.6911	1.703	20.87
Tors 2/pho	.93					
.9993E-01	2.953	1.487	1.285	1.124	1.533	8.004
.1495	2.687	.9680	.6751	.4284	.8149	6.170
.2063	3.393	.7680	.4839	.2789	.5252	5.698
.2502	4.291	.6524	.4084	.3697	.3187	6.647
.2998	5.253	.5717	.3558	.2767	.2850	8.053

TABLE VI.- SPECTRAL CONTENT OF MEASUREMENTS ON ADVANCED BLADE

[Chord and beam are measured in inch-pounds; torsion (Tors) and P-L are presented in pounds]

Mu	1/rev	2/rev	3/rev	4/rev	5/rev	1/2 P-P
Chord 1	.18					
.1005	245.7	42.30	80.00	128.7	40.00	538.0
.1510	281.5	49.06	49.37	110.3	24.51	574.3
.2001	261.7	62.96	62.34	77.90	30.63	433.9
.2516	310.6	112.1	64.41	70.92	19.76	520.4
.2992	297.5	190.0	95.72	101.8	28.03	620.8
Chord 2	.28					
.1005	204.0	43.24	118.3	137.1	55.85	548.9
.1510	248.5	61.87	74.02	111.5	27.94	576.8
.2001	249.4	81.06	84.27	74.89	33.68	460.3
.2516	290.1	142.9	83.14	68.19	20.30	522.0
.2992	284.3	255.0	129.1	100.4	27.07	687.2
Chord 3	.47					
.1005	127.6	48.85	78.77	141.6	30.50	450.8
.1510	174.8	73.94	53.90	122.3	15.67	504.4
.2001	198.2	87.31	63.79	83.55	18.93	438.1
.2516	245.8	131.0	65.17	83.67	13.38	472.0
.2992	248.6	215.2	97.97	99.09	14.49	603.2
Beam 1	.18					
.1005	21.54	37.85	130.2	165.2	54.77	475.4
.1510	10.50	29.56	79.05	123.5	17.43	320.7
.2001	21.83	59.44	71.08	97.24	14.28	261.1
.2516	54.15	279.9	134.5	172.4	31.03	596.1
.2992	91.93	492.7	134.7	205.4	60.21	877.0
Beam 2	.28					
.1005	29.59	28.86	94.86	103.9	28.78	292.5
.1510	32.04	33.39	55.63	79.38	10.67	170.5
.2001	53.91	55.63	48.32	62.27	9.254	170.7
.2516	67.35	122.4	44.07	55.77	9.152	228.9
.2992	85.95	212.2	43.85	66.05	17.25	365.4
Beam 3	.47					
.1005	40.14	30.77	46.41	15.69	11.18	141.9
.1510	53.25	48.74	33.31	13.52	1.940	141.2
.2001	85.01	63.12	29.67	12.28	4.026	183.4
.2516	110.1	107.5	30.06	9.821	6.607	254.9
.2992	144.1	191.6	39.84	7.308	8.726	385.2
Beam 4	.60					
.1005	48.10	45.88	25.14	73.31	26.82	201.9
.1510	69.93	66.74	23.86	55.15	10.77	228.9
.2001	111.9	81.93	25.85	42.29	8.295	272.7
.2516	71.95	58.74	11.25	17.76	4.467	168.7
.2992	86.49	94.12	15.51	15.37	8.930	214.4
Beam 5	.77					
.1005	36.95	45.09	12.88	76.89	19.74	211.3
.1510	57.01	50.94	5.826	56.60	11.69	201.0
.2001	84.86	52.64	8.337	45.32	9.453	211.9
.2516	104.4	69.49	7.619	32.61	3.745	219.7
.2992	122.1	116.2	9.994	39.27	11.09	287.5

TABLE VI.- Concluded

Mu	1/rev	2/rev	3/rev	4/rev	5/rev	1/2 P-P
P-L	.05					
.1005	7.209	7.548	3.444	9.146	3.695	30.04
.1510	4.713	8.196	3.346	6.287	2.810	23.84
.2001	6.253	10.99	3.351	3.822	2.177	25.16
.2516	10.66	15.12	3.389	2.167	1.324	31.81
.2992	16.17	18.82	11.37	3.864	1.266	49.94
Tors 1/pho	.18					
.1005	4.801	7.919	3.114	8.768	1.431	26.68
.1510	4.783	7.889	3.165	6.301	1.086	21.06
.2001	7.846	9.914	2.277	3.908	1.214	21.85
.2516	13.22	15.81	3.003	3.019	.5925	33.05
.2992	18.73	21.89	10.30	2.692	2.546	47.36
Tors 2/phc	.77					
.1005	1.399	2.533	2.324	1.589	.9369	8.067
.1510	4.279	1.226	2.292	1.615	.3659	10.18
.2001	6.382	2.221	1.636	1.675	.5482	13.11
.2516	9.265	4.810	1.071	1.958	.4230	17.99
.2992	11.54	8.212	1.970	1.998	.6718	23.94
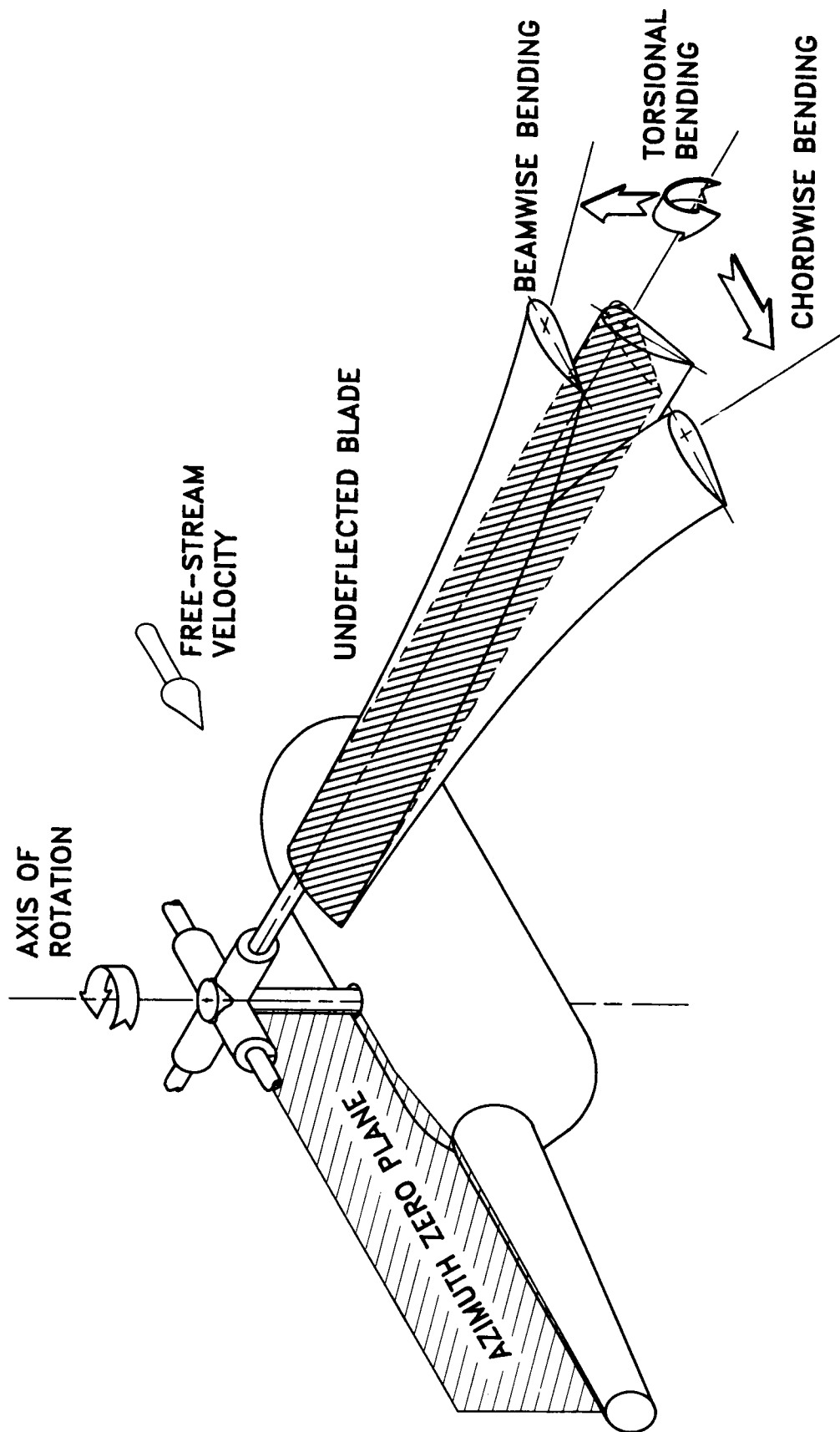
Figure 1.- Reference axis for blade bending measurements.

L-84-2433

Figure 2.- Model installed in the Langley 14- by 22-Foot Subsonic Tunnel.
Baseline blades installed.
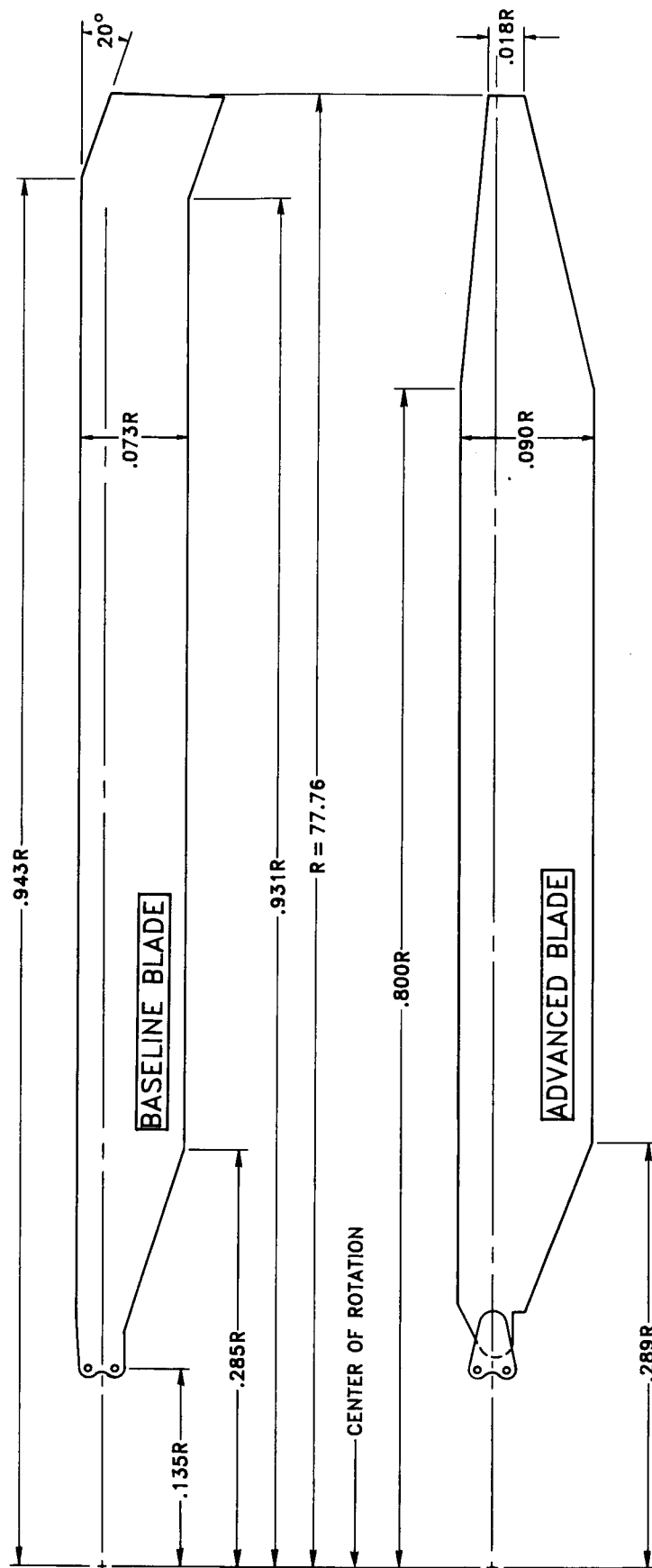
Figure 3.- Scaled rotor blade planforms. Linear dimensions are given in inches.

18
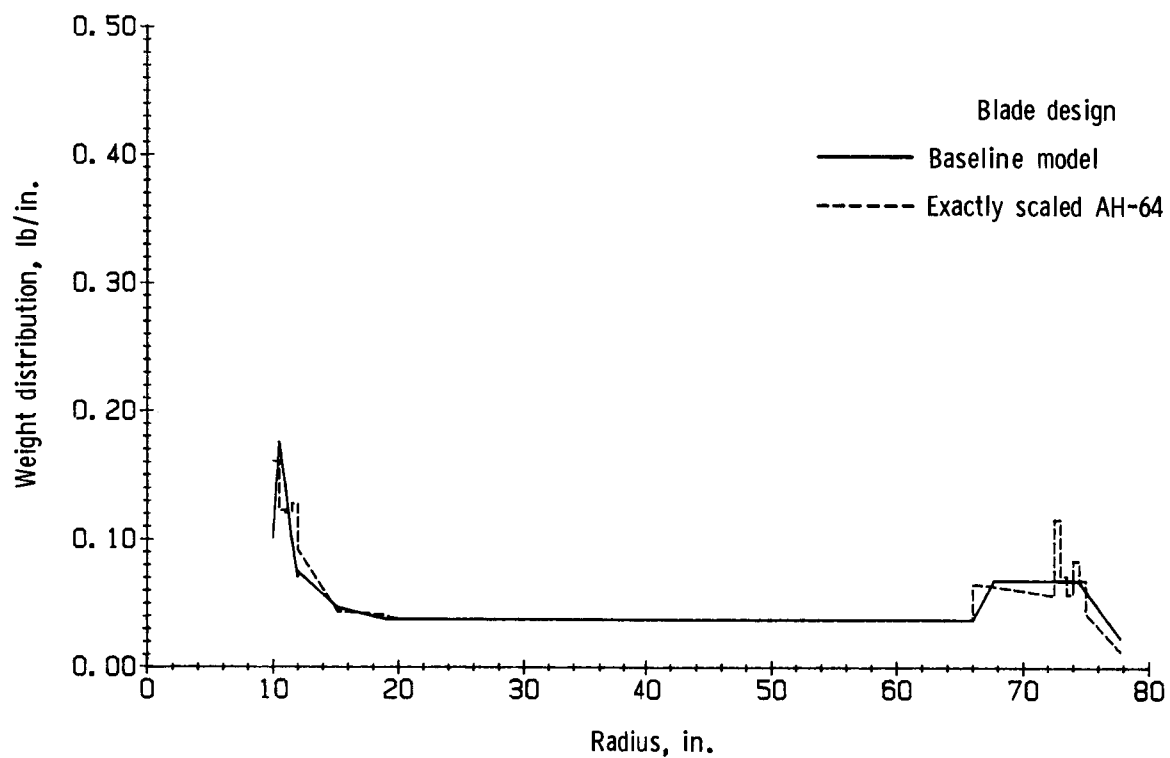
(a) Weight distribution.
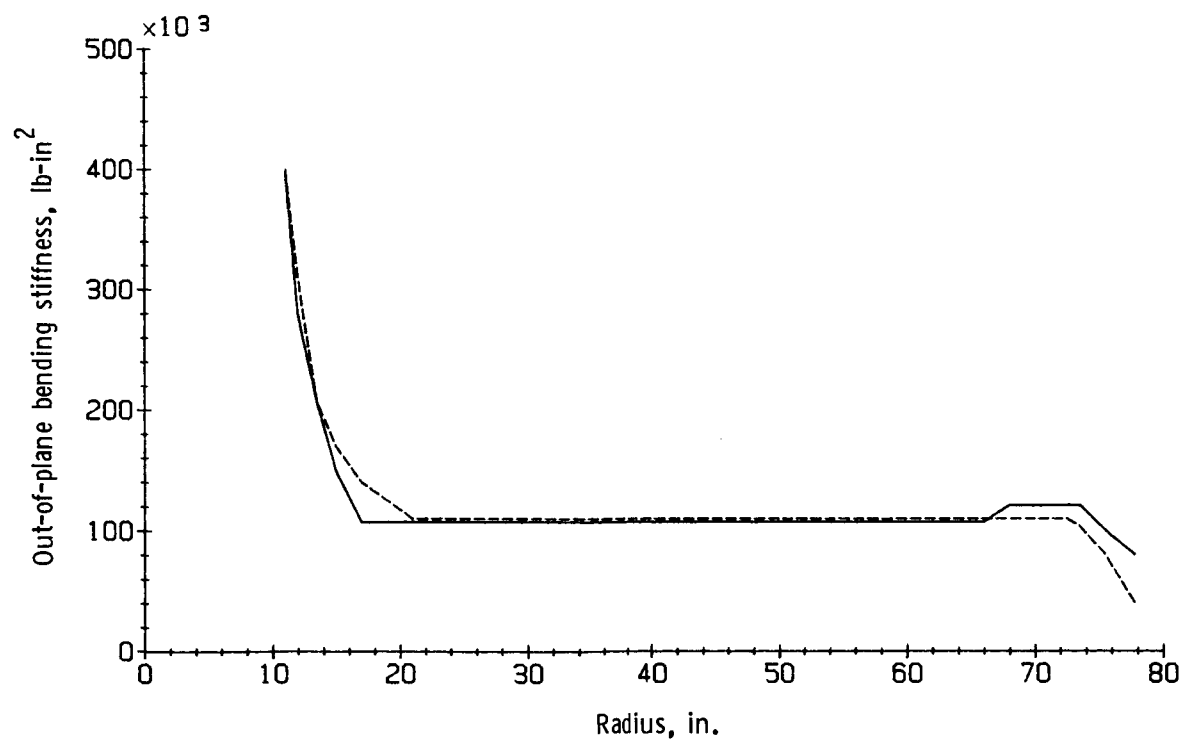
(b) Out-of-plane bending stiffness.

Figure 4.- Sectional property distribution of baseline blade.
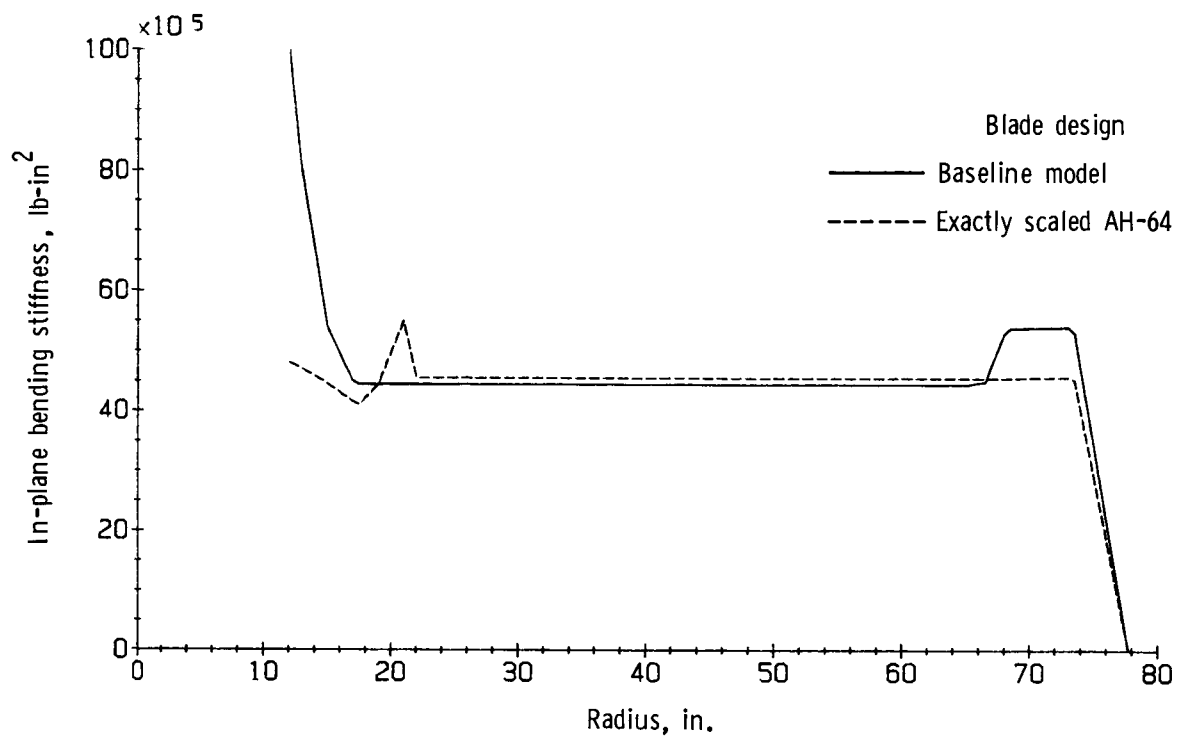
(c) In-plane bending stiffness.
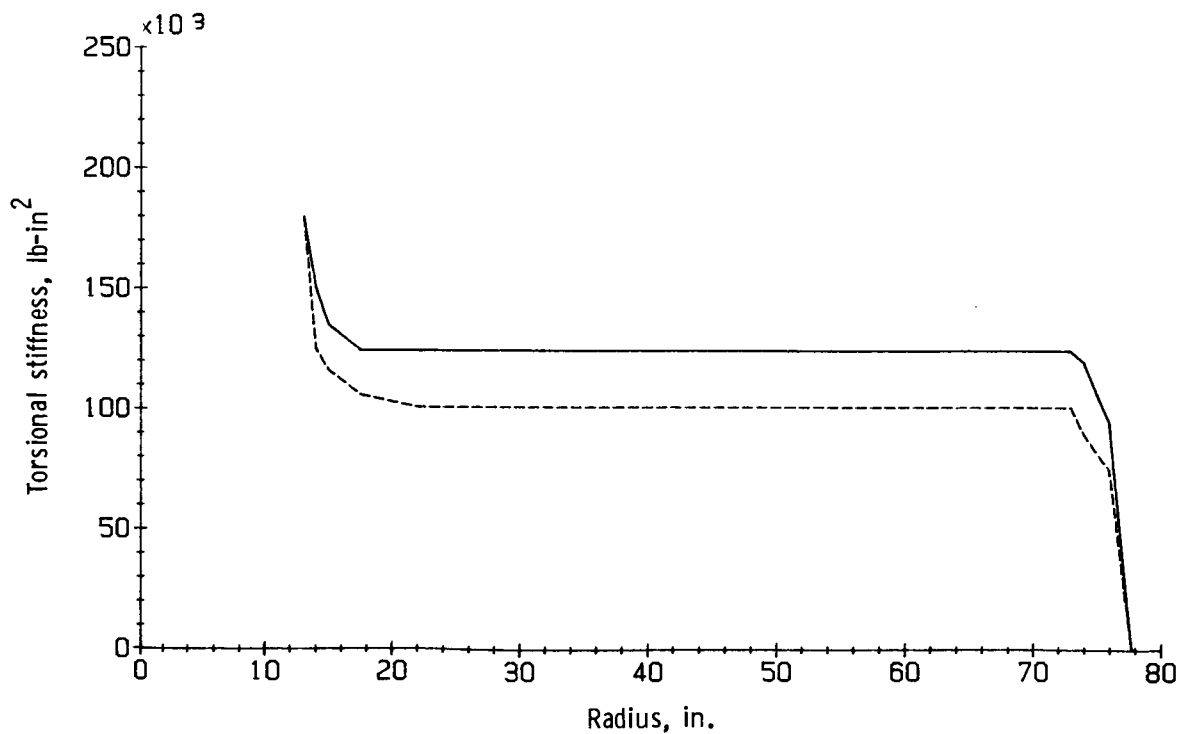
(d) Torsional stiffness.

Figure 4.- Concluded.
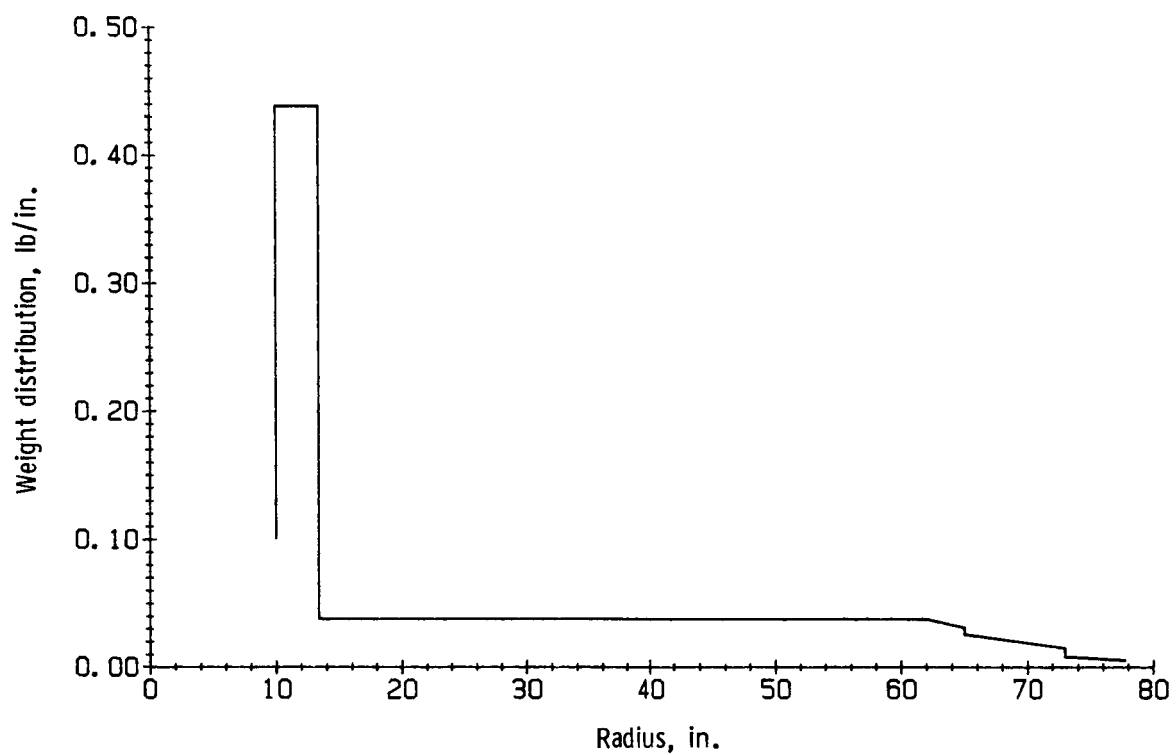
(a) Weight distribution.
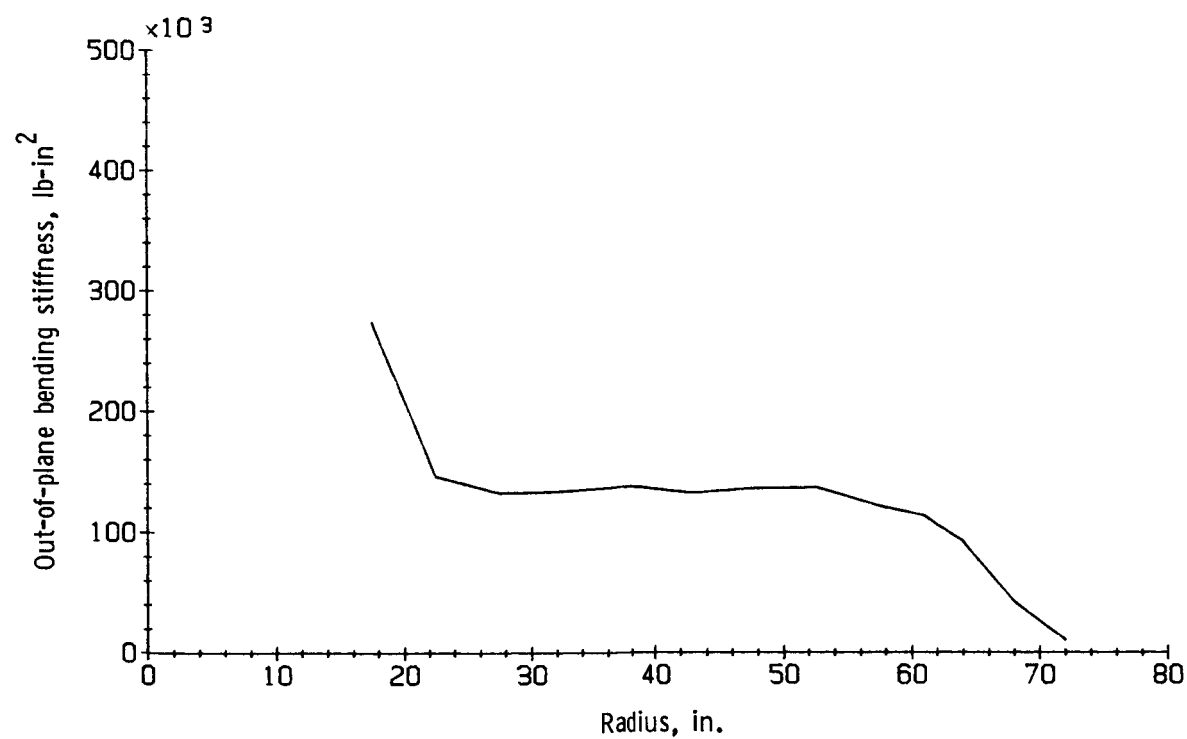
(b) Out-of-plane bending stiffness.

Figure 5.- Sectional property distribution of advanced blade.
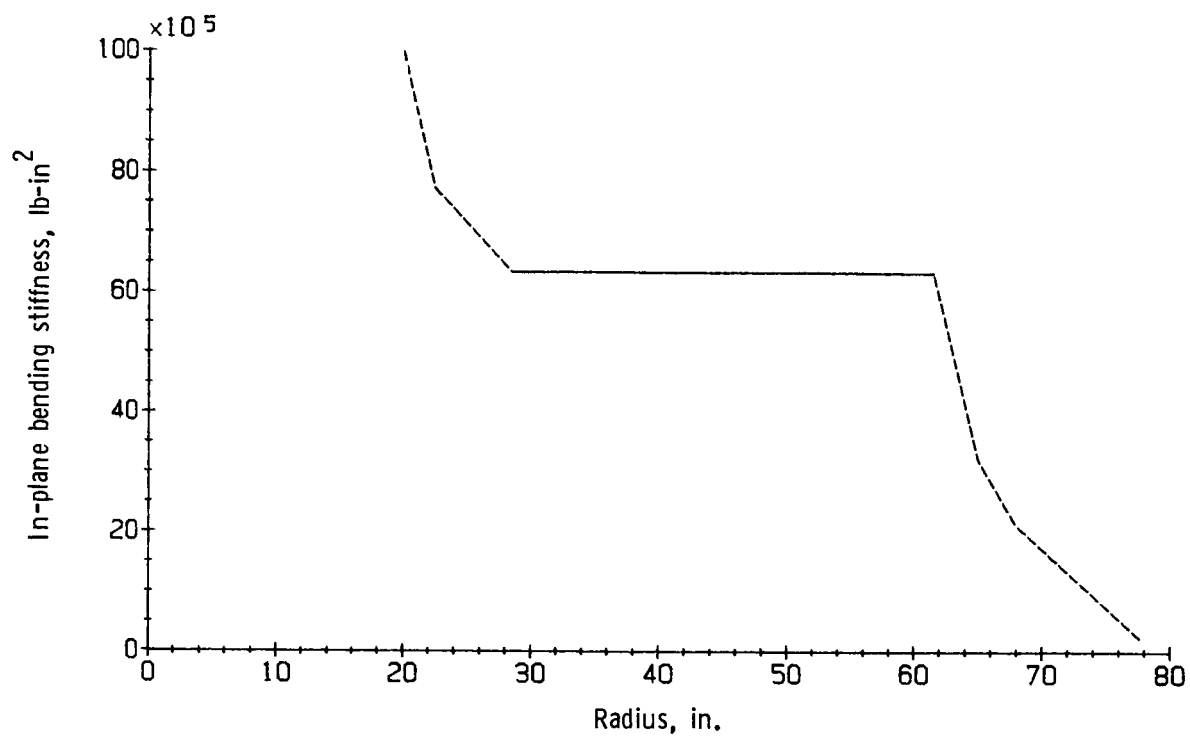
(c) In-plane bending stiffness.
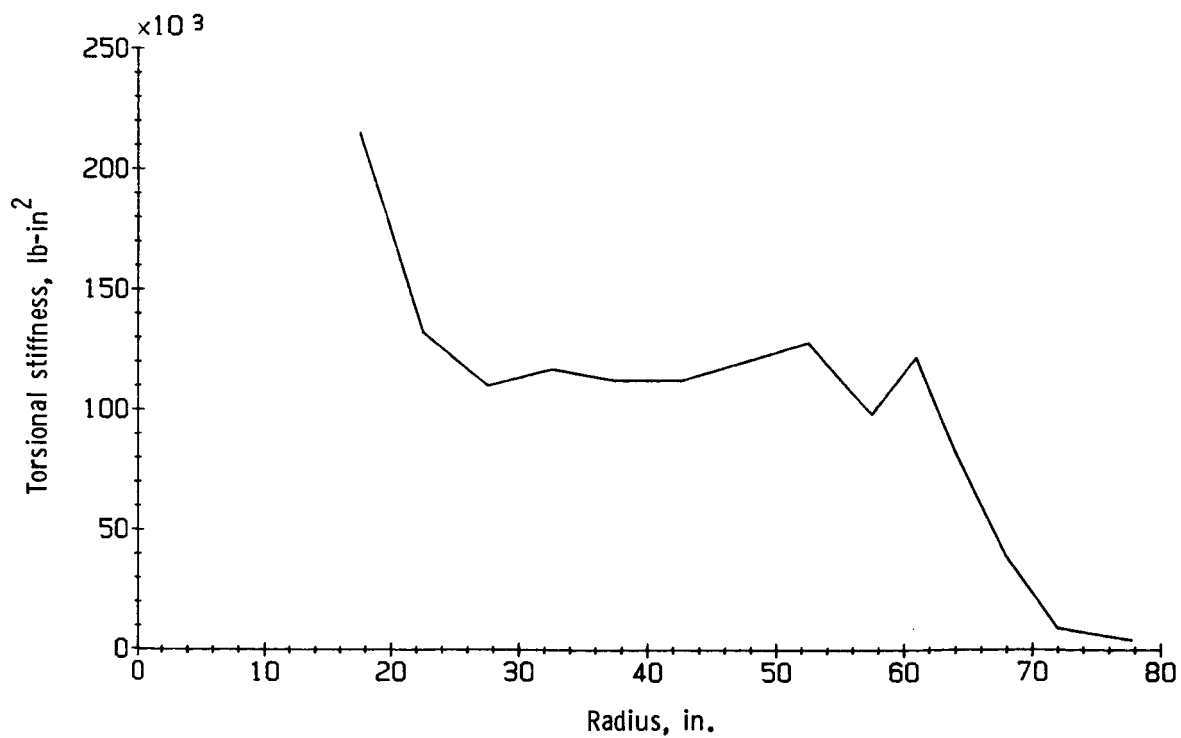
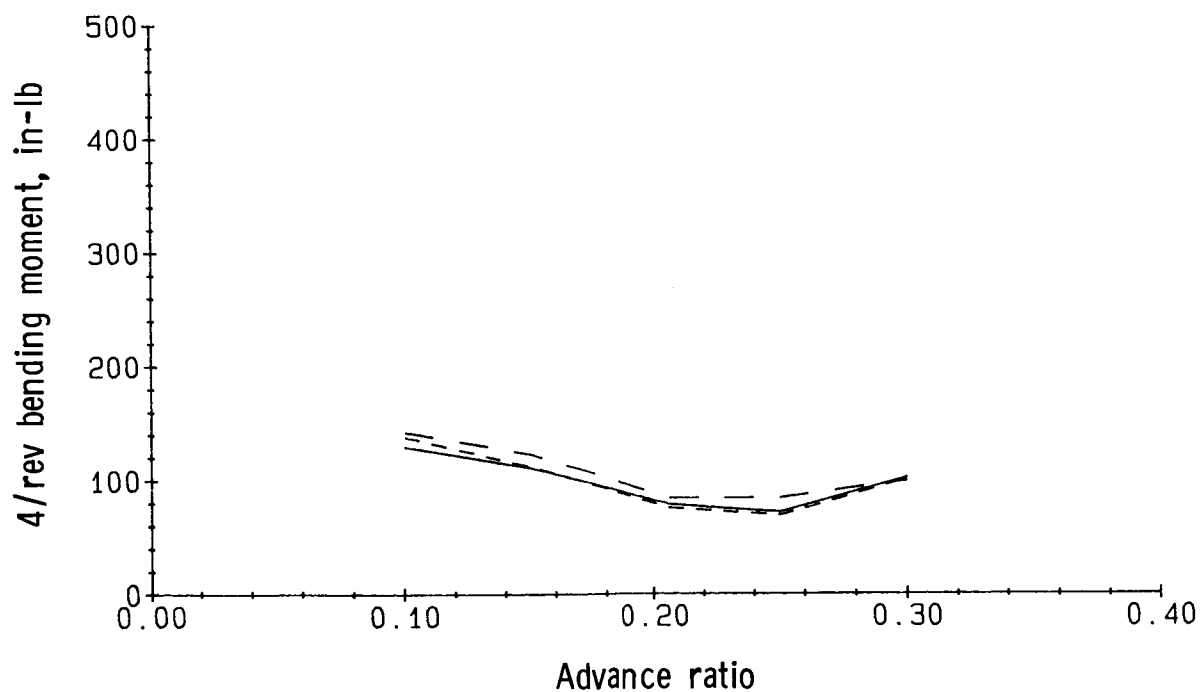(d) Torsional stiffness.

Figure 5.- Concluded.
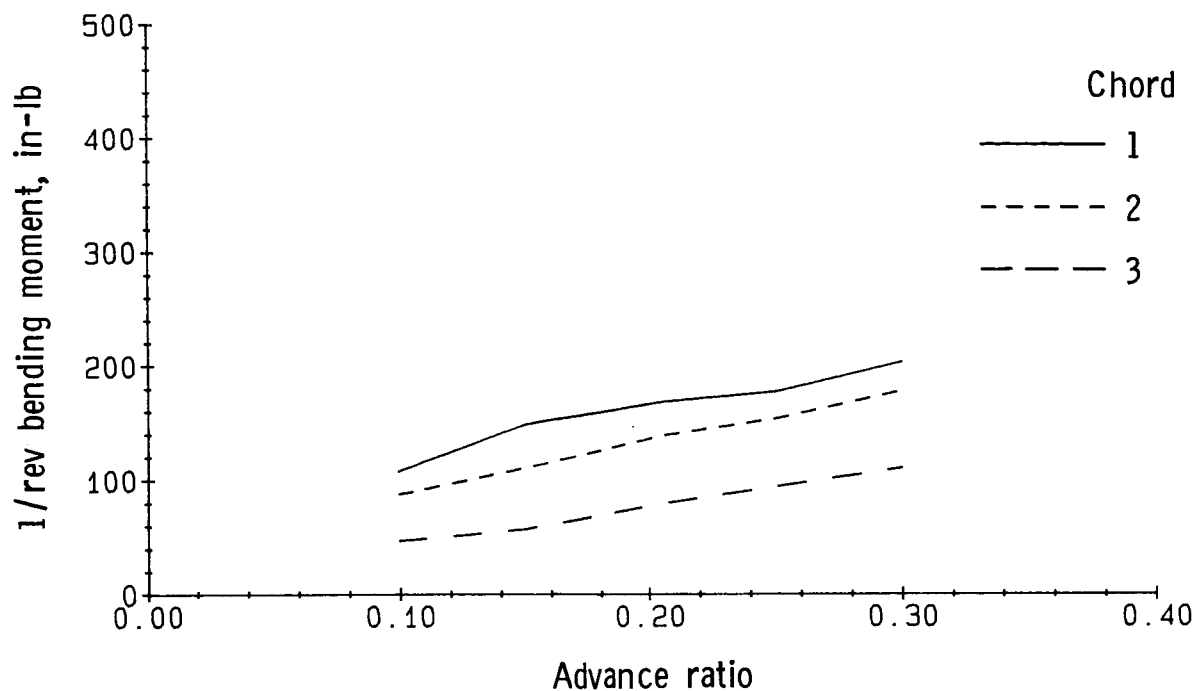
(a) 1/rev bending moment.
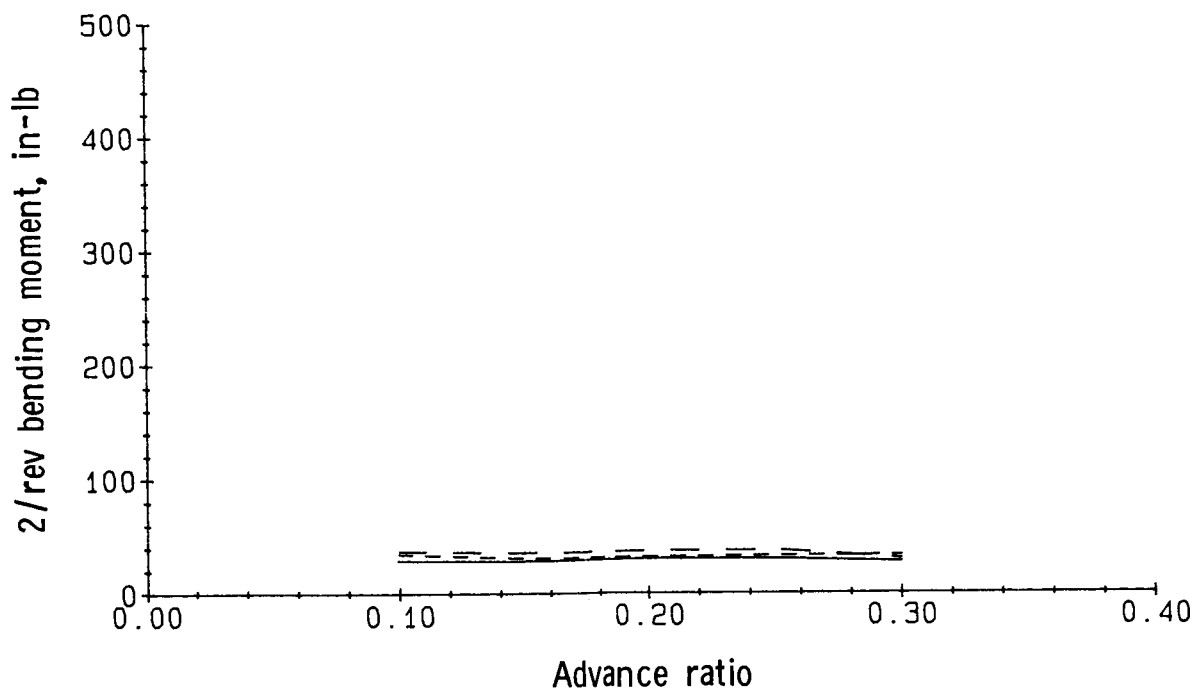
(b) 2/rev bending moment.

Figure 6.- Chord bending moment of baseline blade.
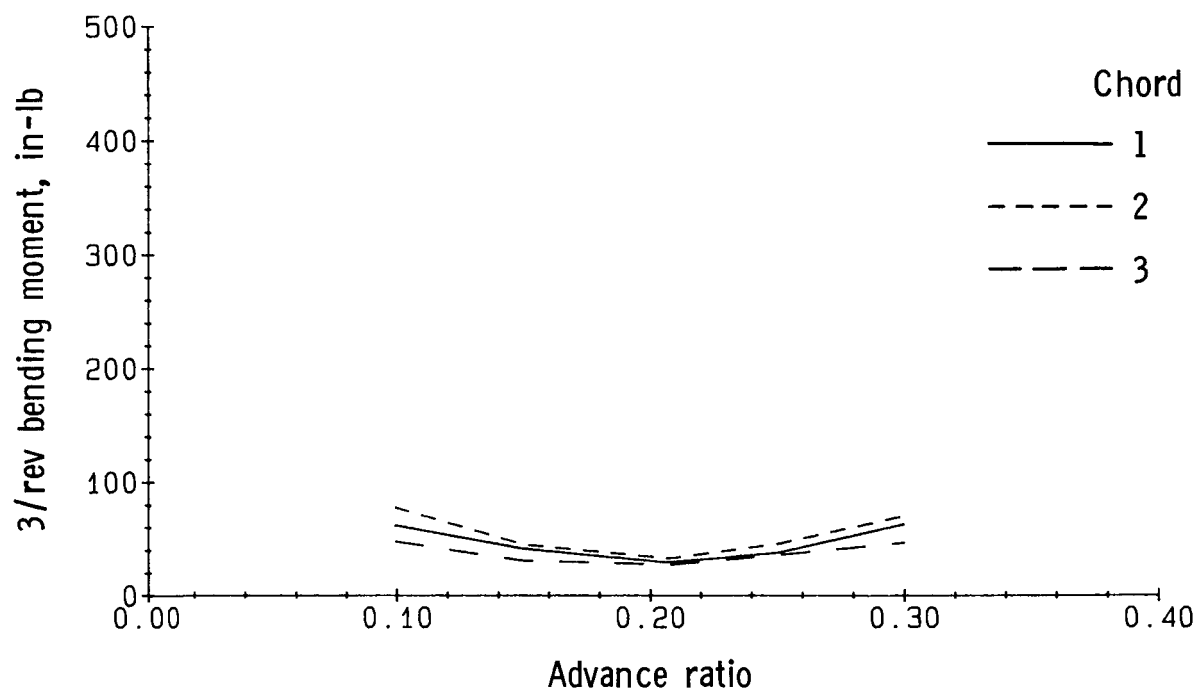
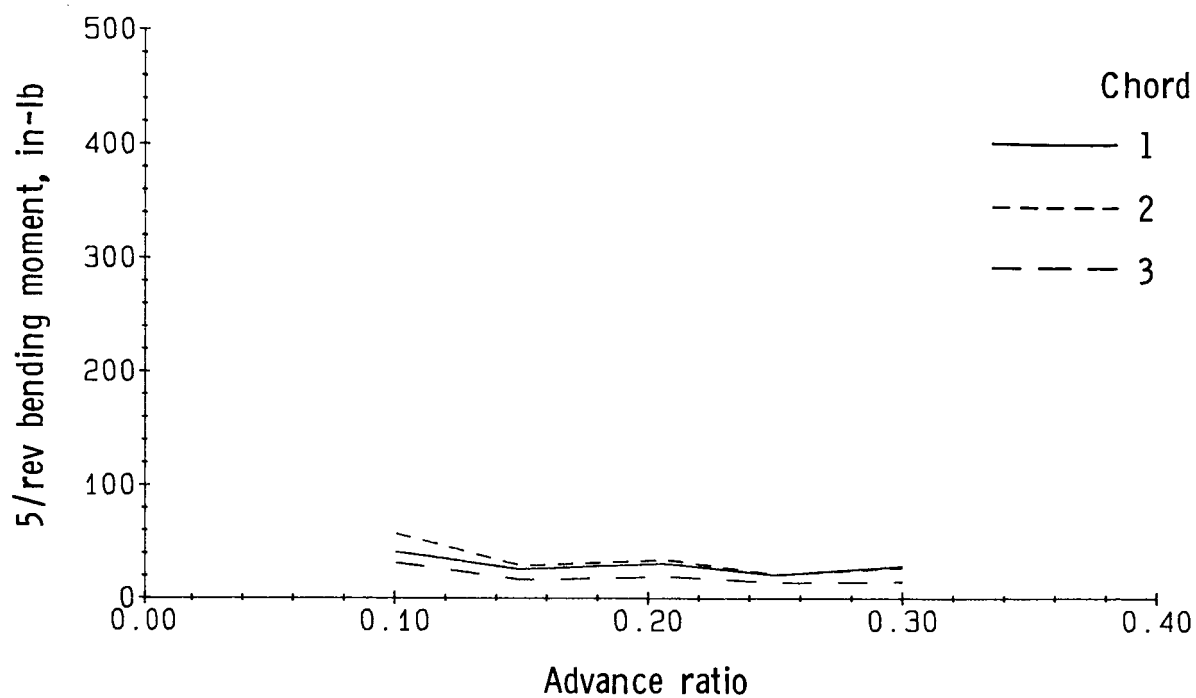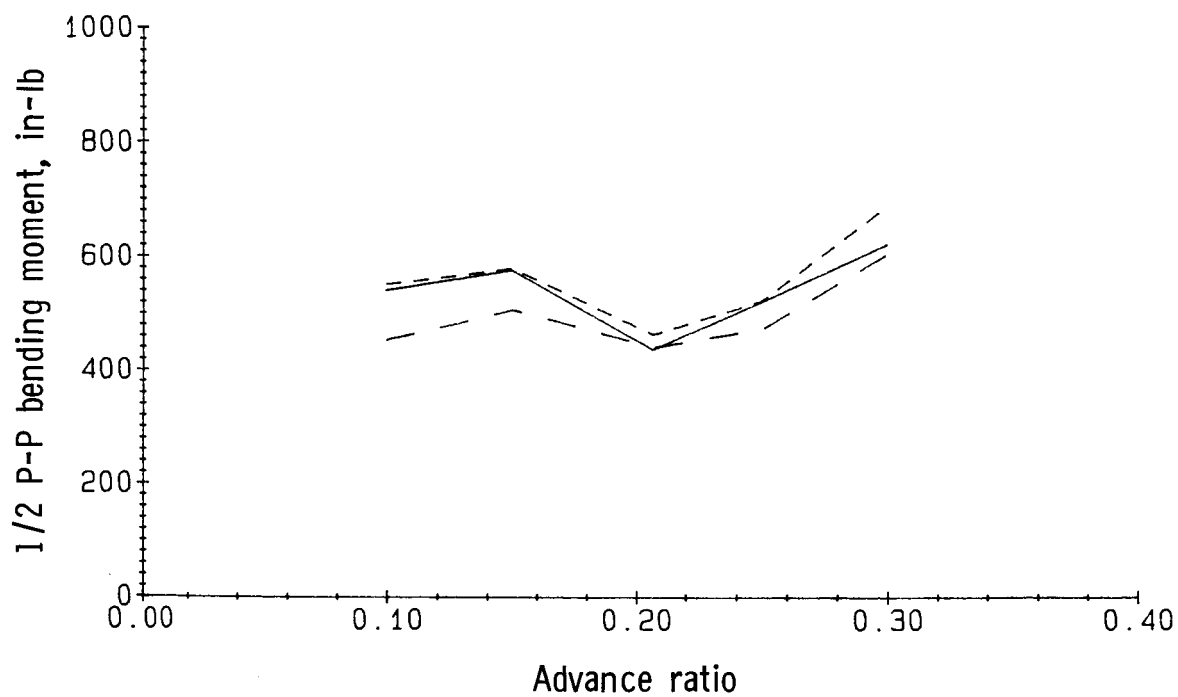(c) 3/rev bending moment.
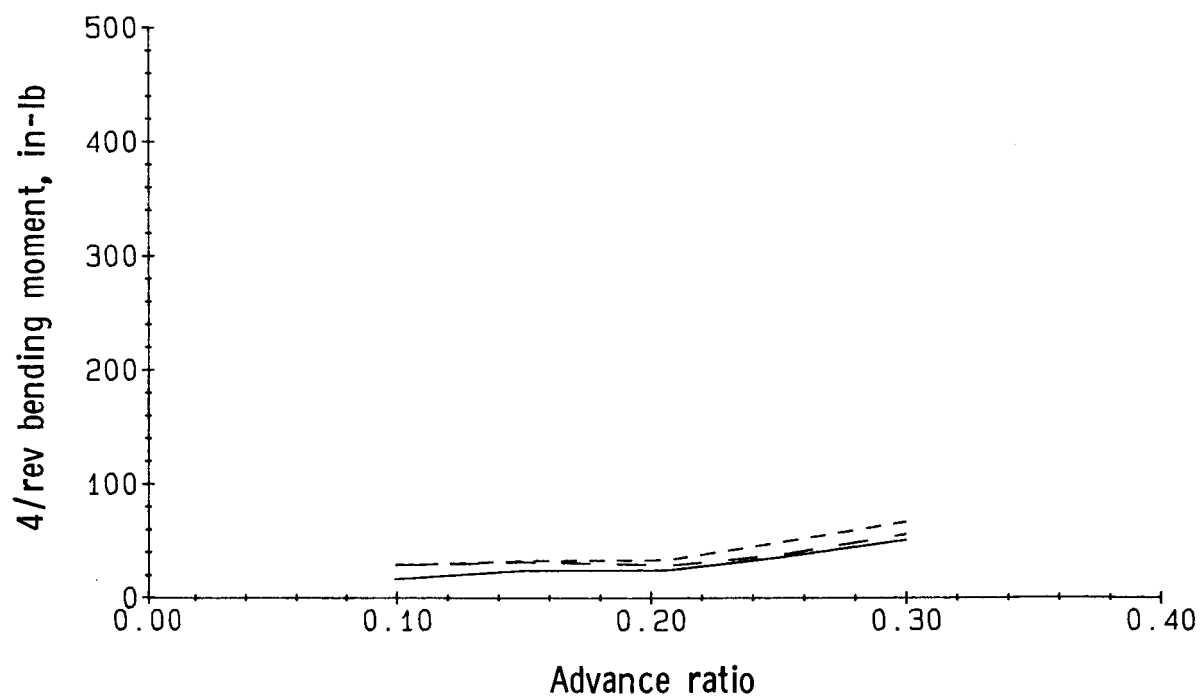
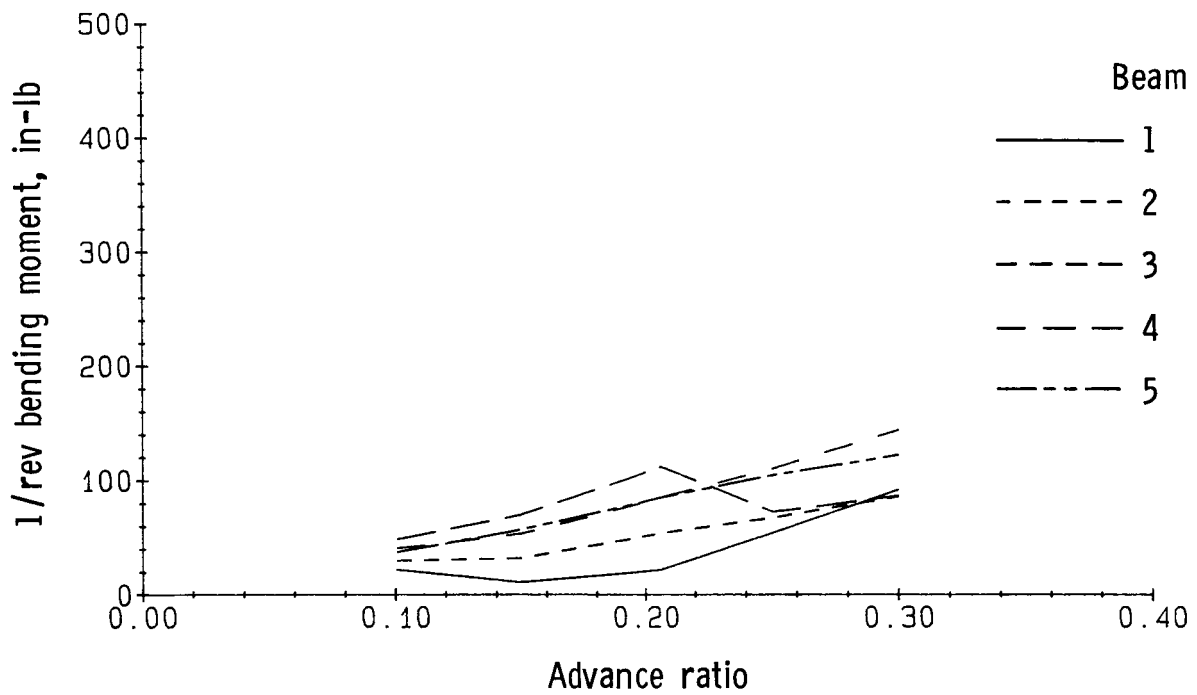(d) 4/rev bending moment.
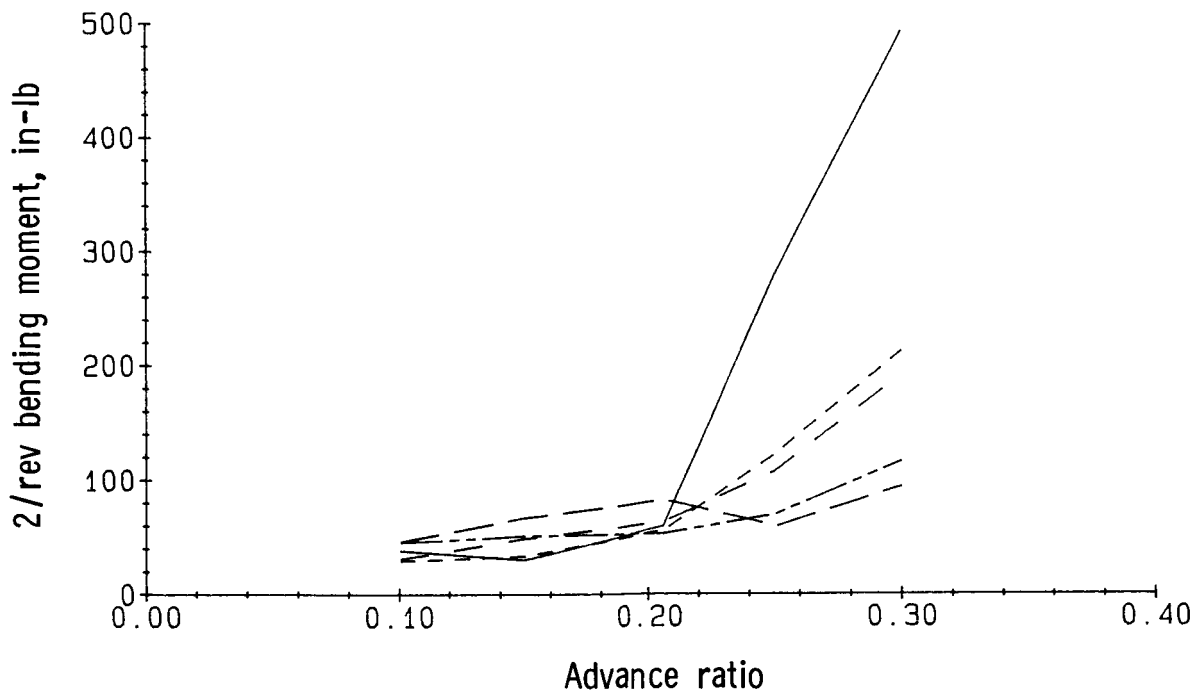
Figure 6.- Continued.
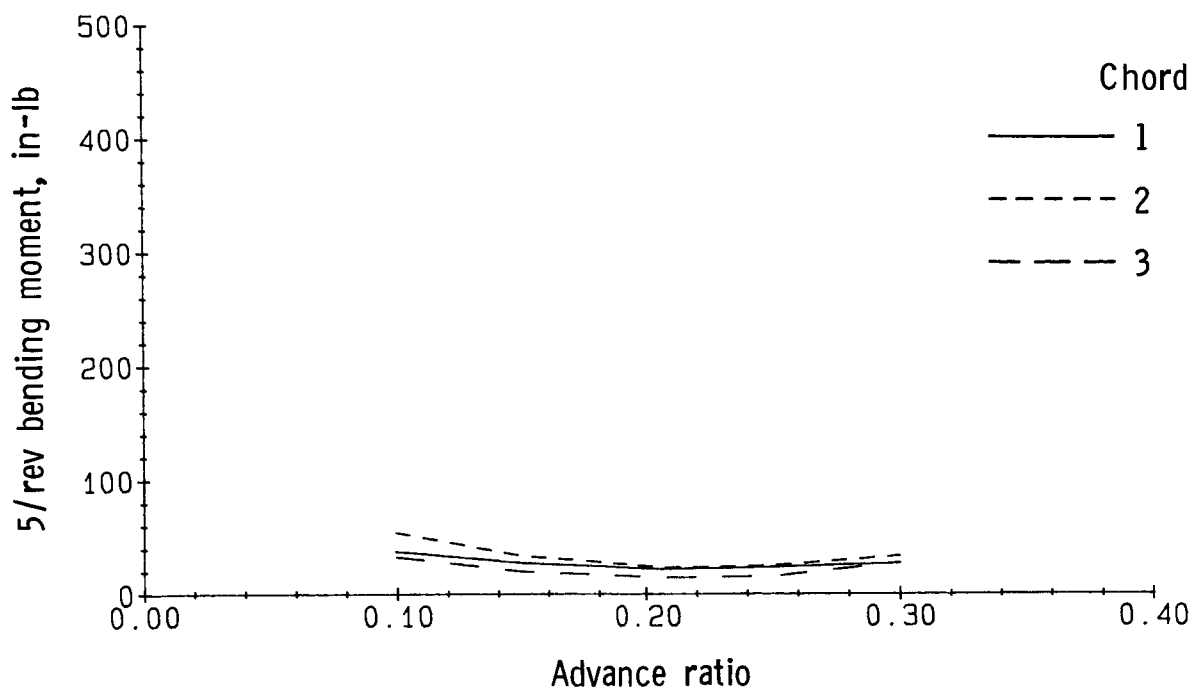
(e) 5/rev bending moment.
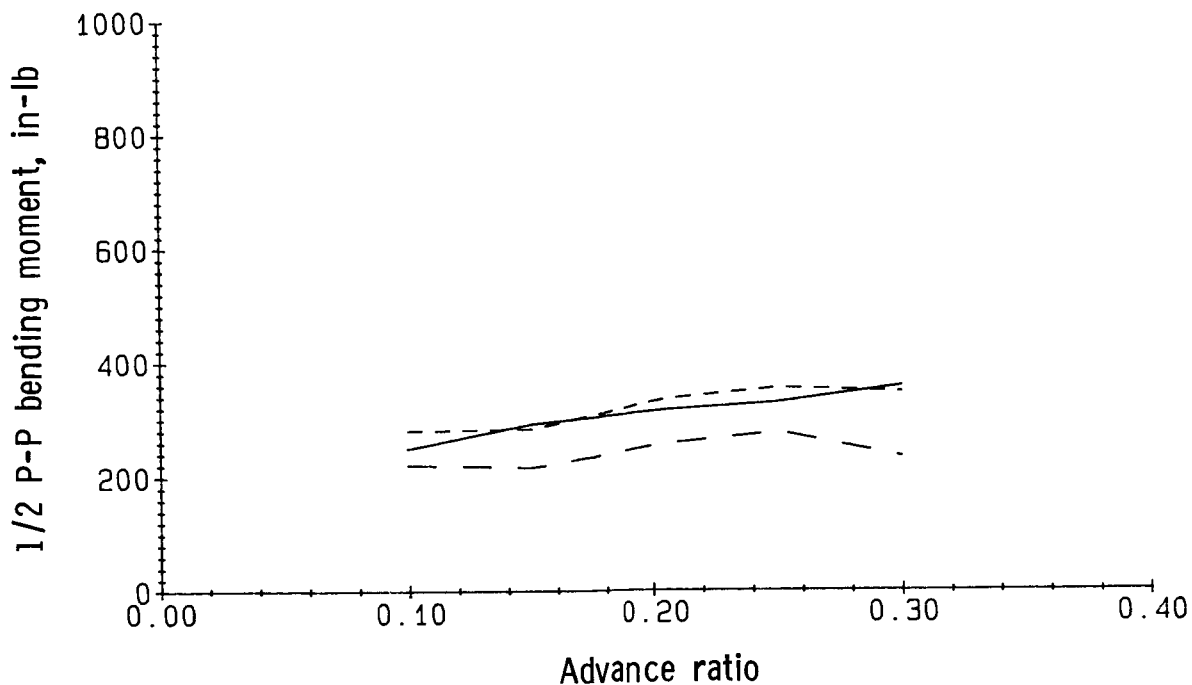
(f) 1/2 peak-to-peak bending moment.

Figure 6.- Concluded.
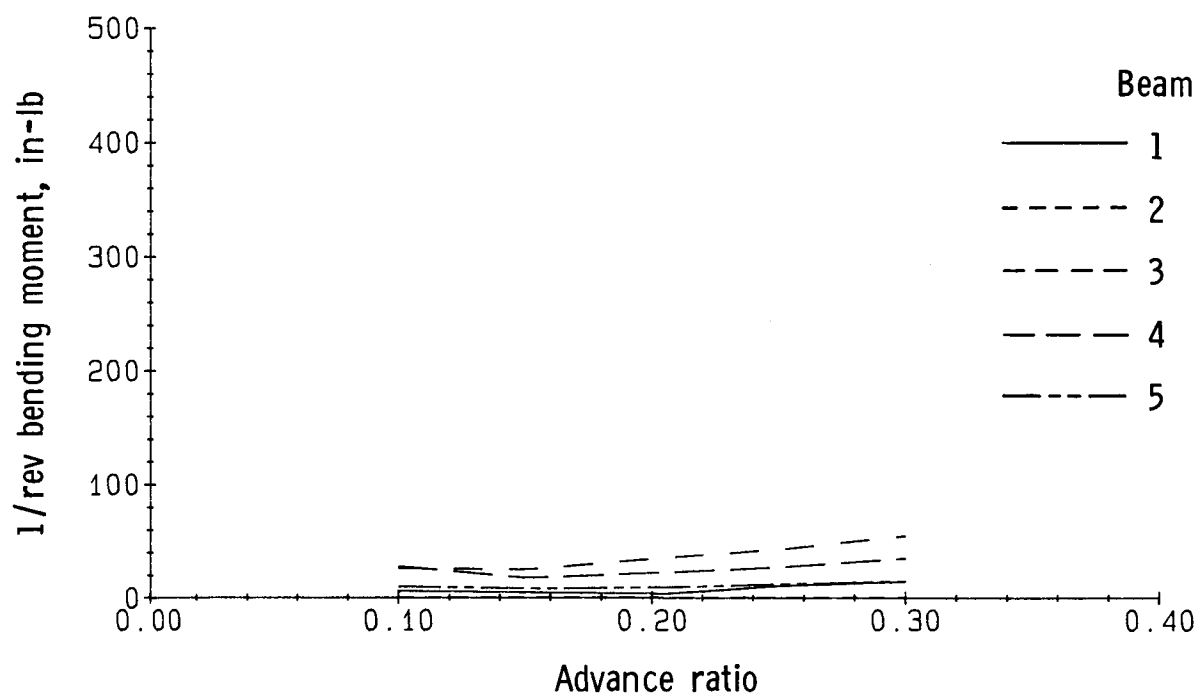
(a) 1/rev bending moment.
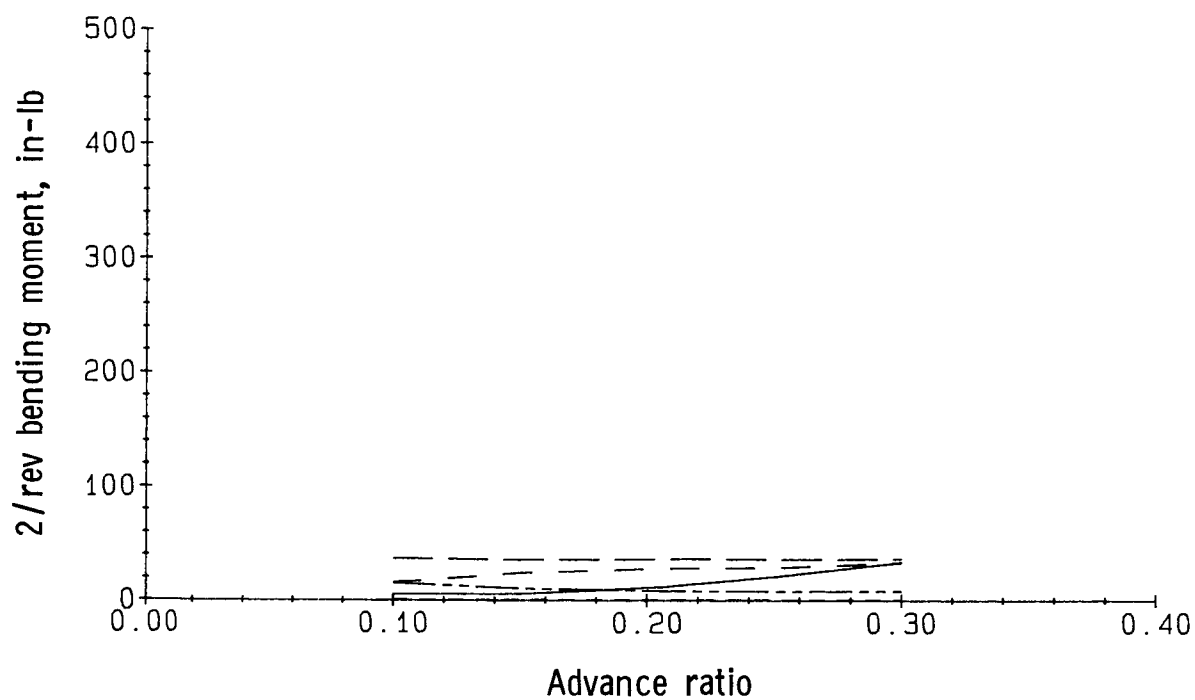
(b) 2/rev bending moment.

Figure 7.- Beam bending moment of baseline blade.
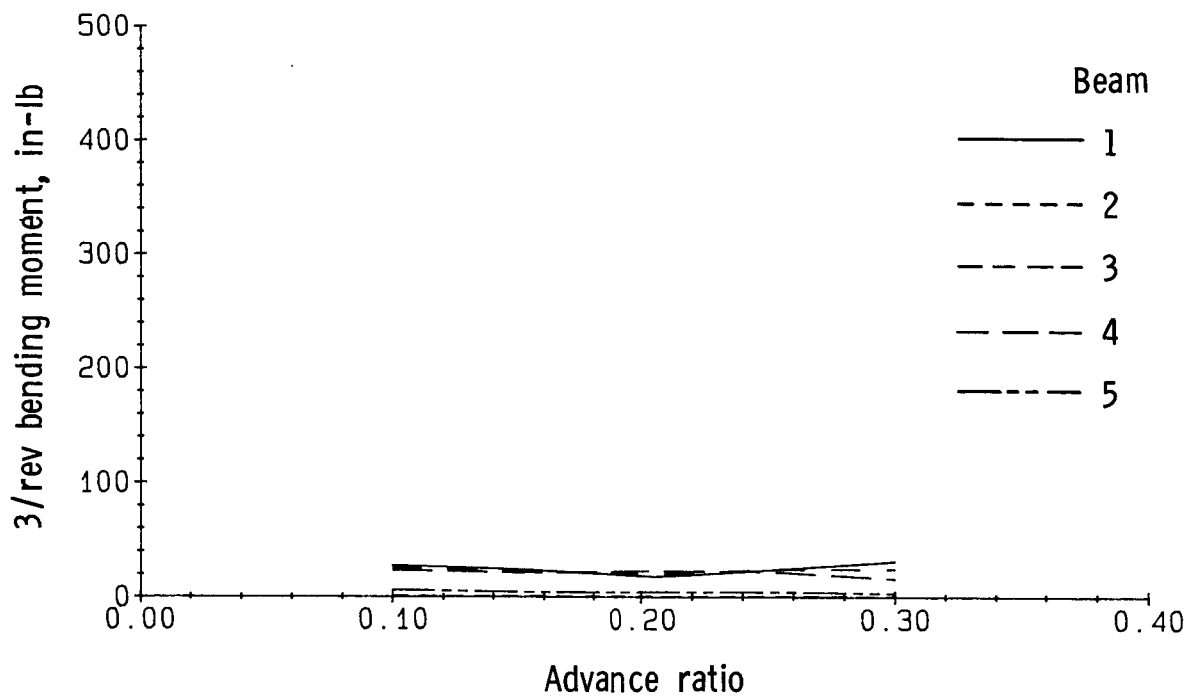
(c) 3/rev bending moment.
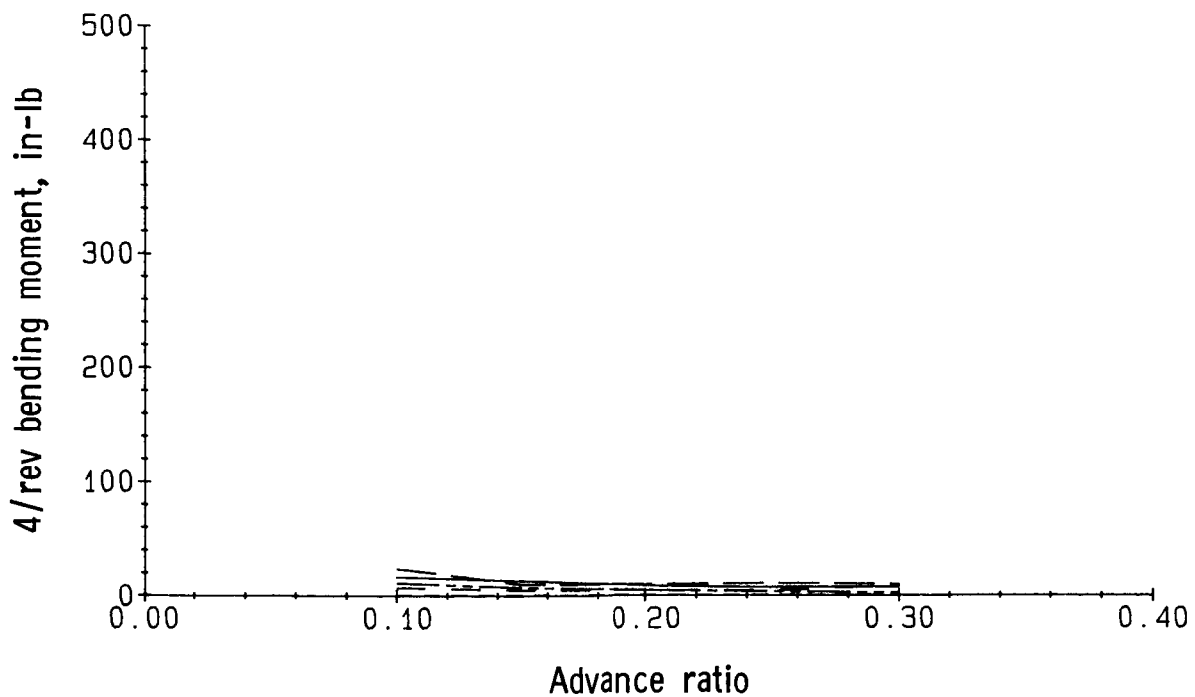
(d) 4/rev bending moment.

Figure 7.- Continued.
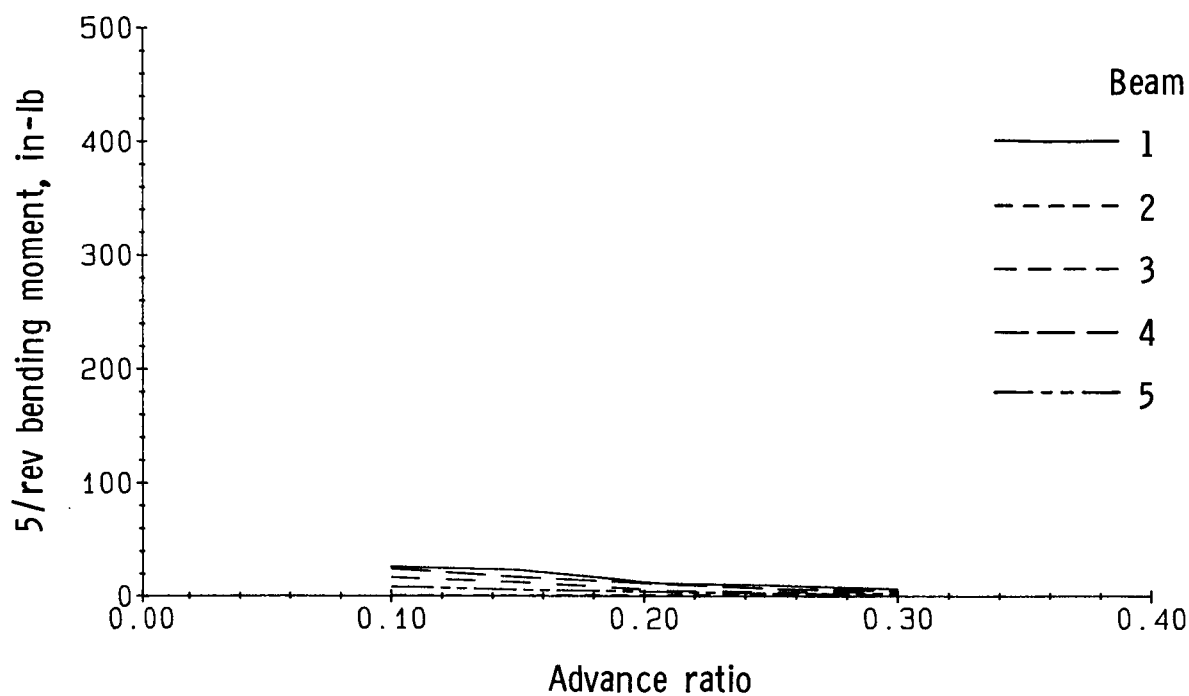
(e) 5/rev bending moment.
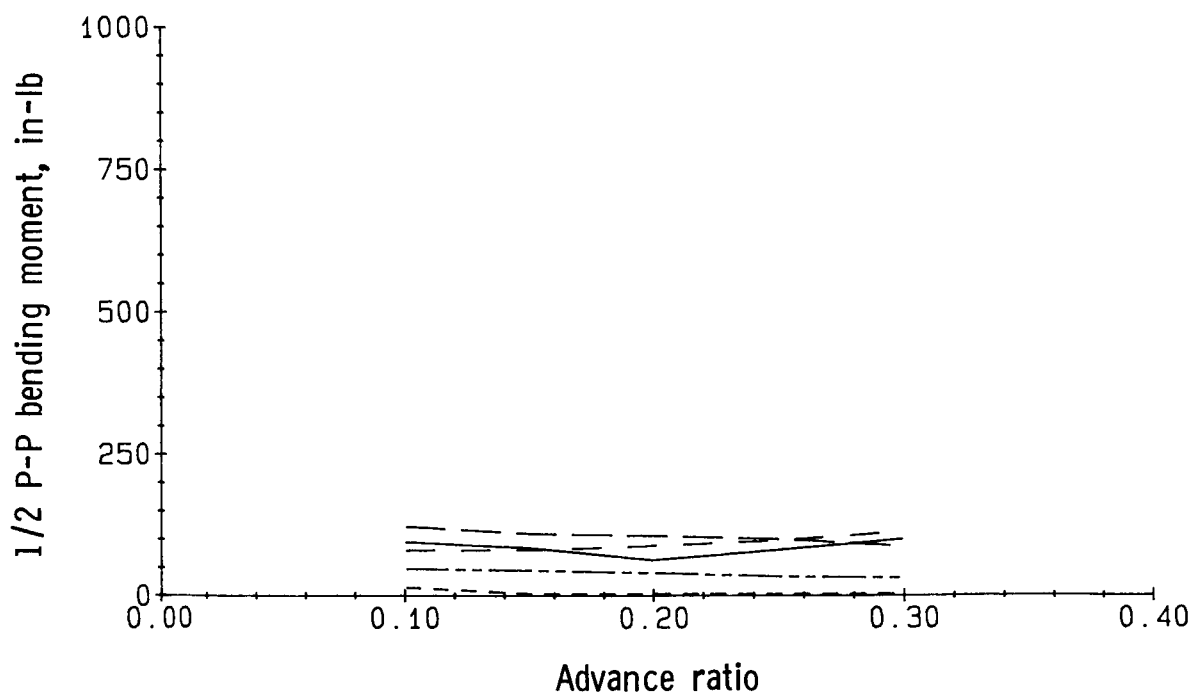
(f) 1/2 peak-to-peak bending moment.

Figure 7.- Concluded.

28
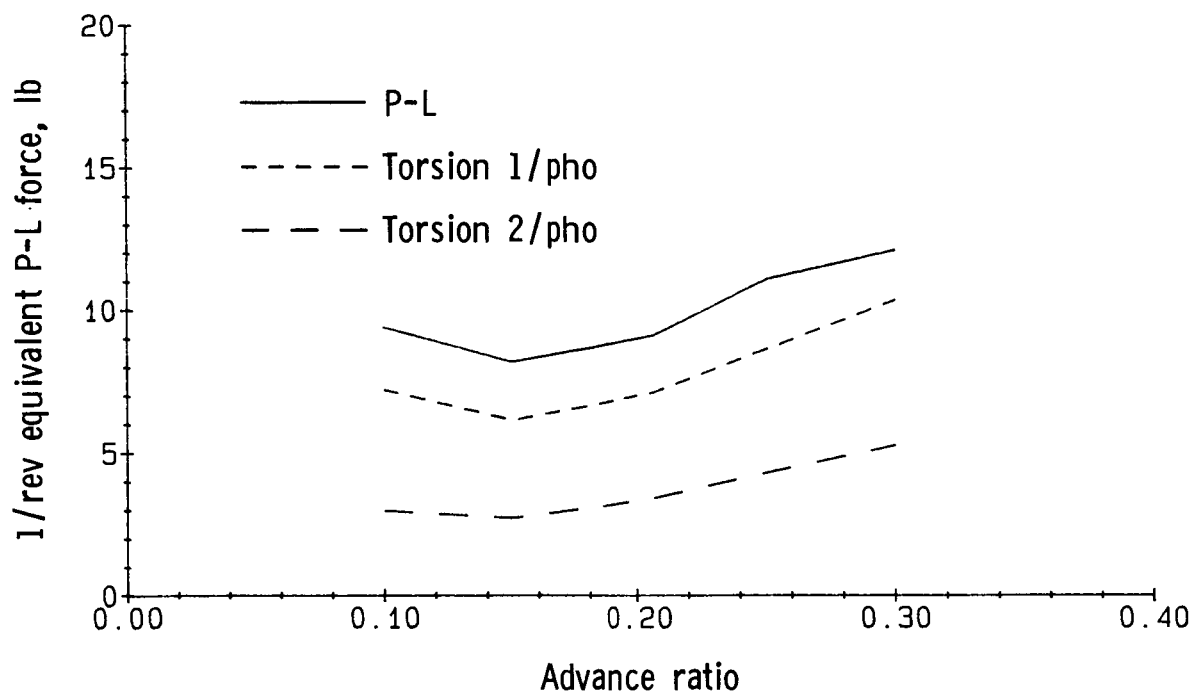
(a) 1/rev equivalent pitch-link force.

(b) 2/rev equivalent pitch-link force.

Figure 8.- Equivalent pitch-link forces of baseline blade.
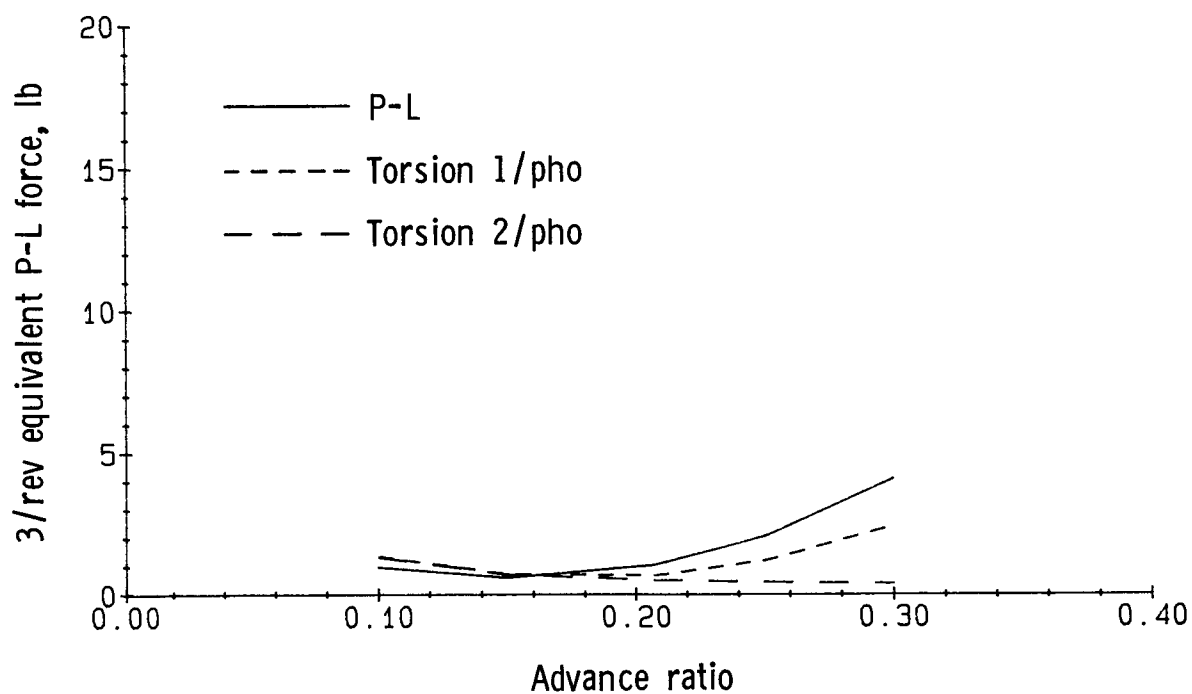
(c) 3/rev equivalent pitch-link force.
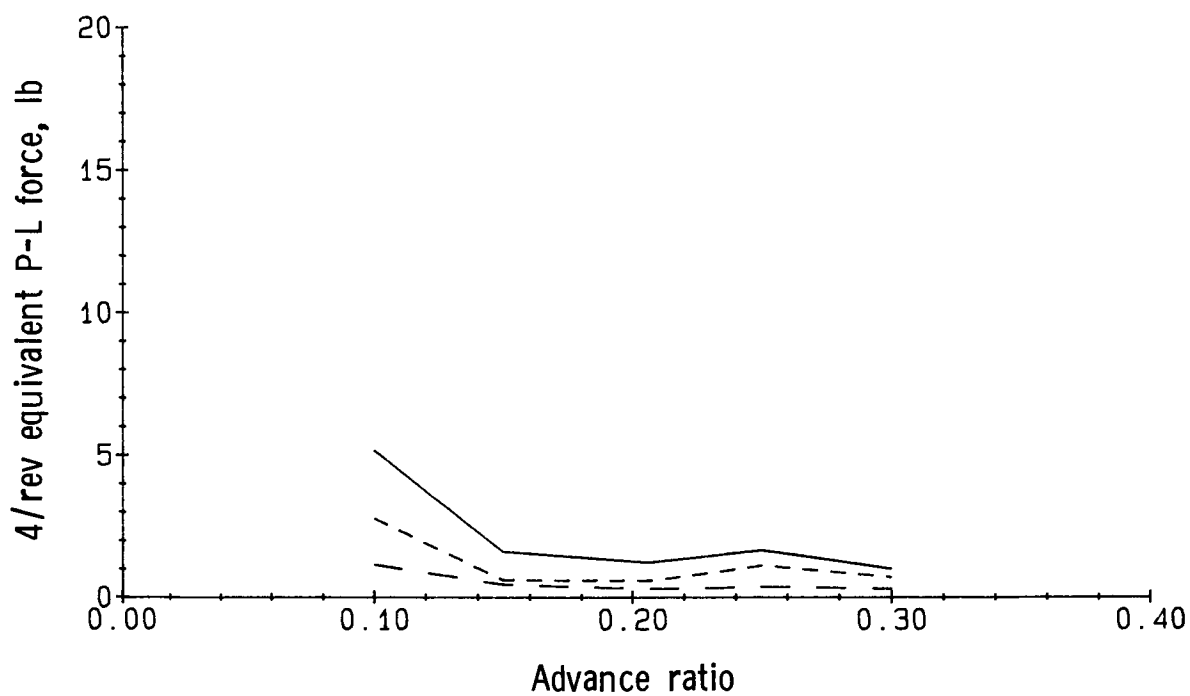
(d) 4/rev equivalent pitch-link force.

Figure 8.- Continued.
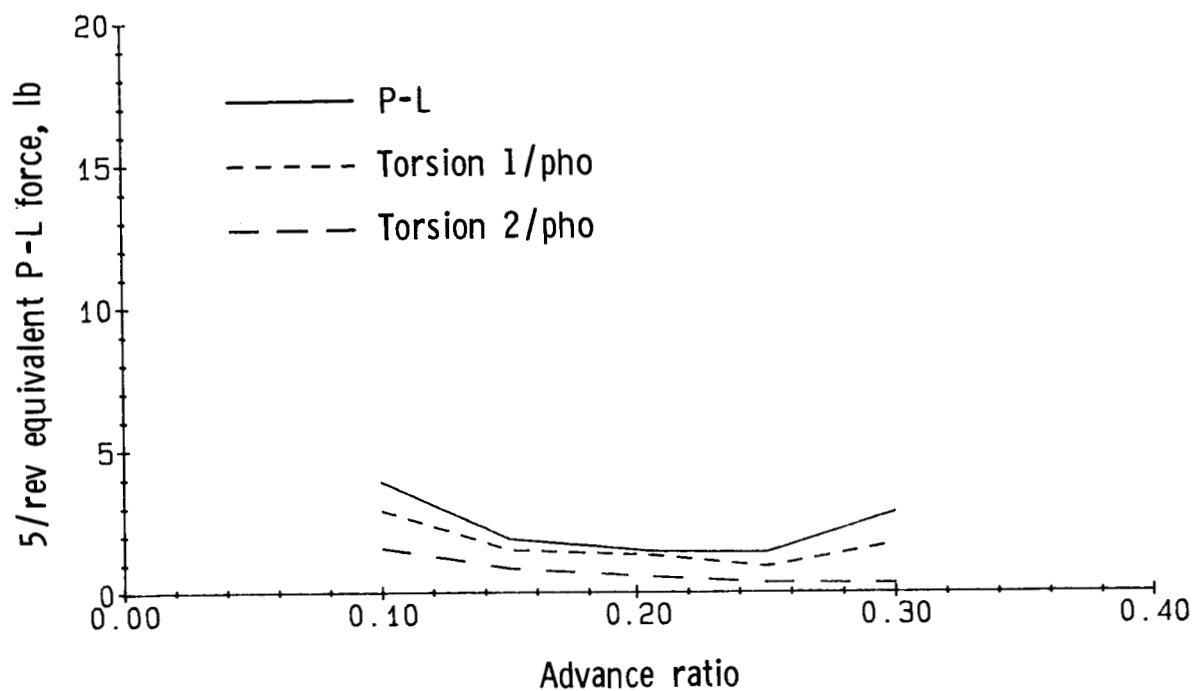
(e) 5/rev equivalent pitch-link force.
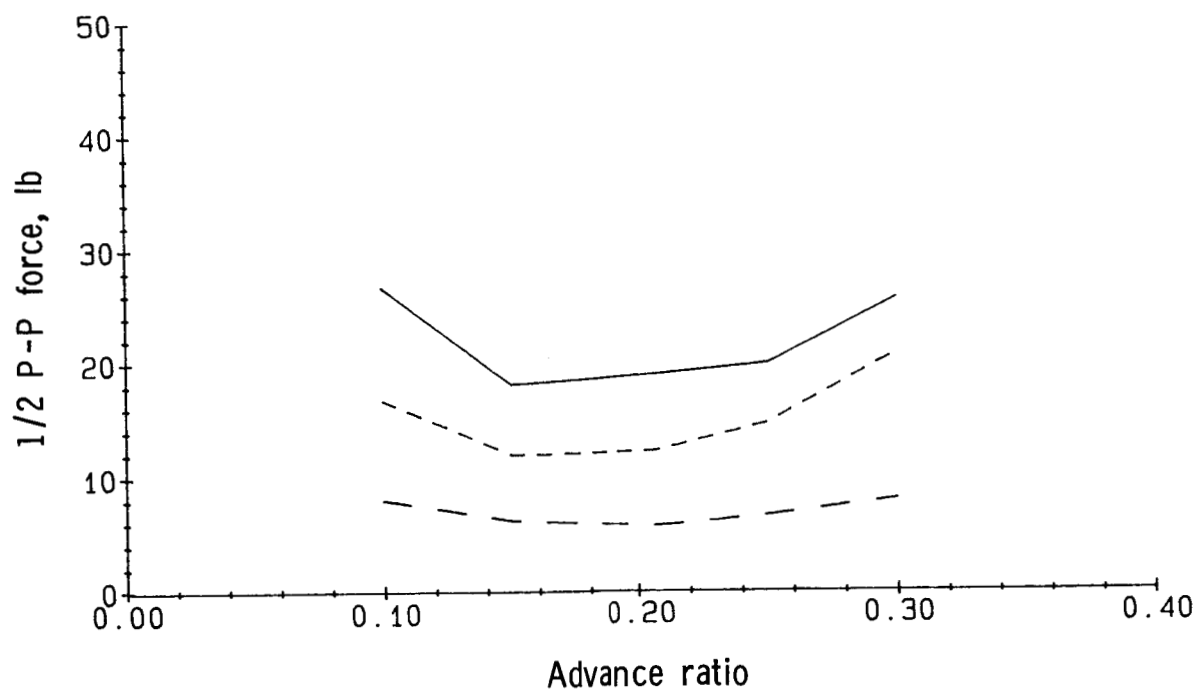
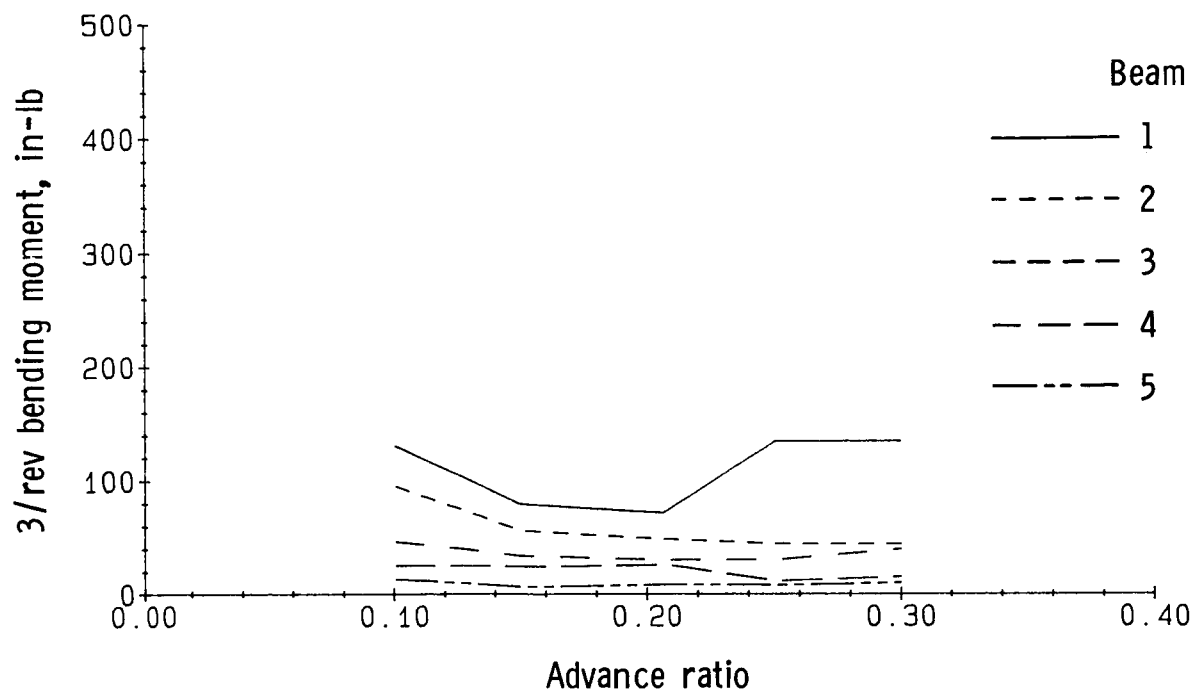(f) 1/2 peak-to-peak force.
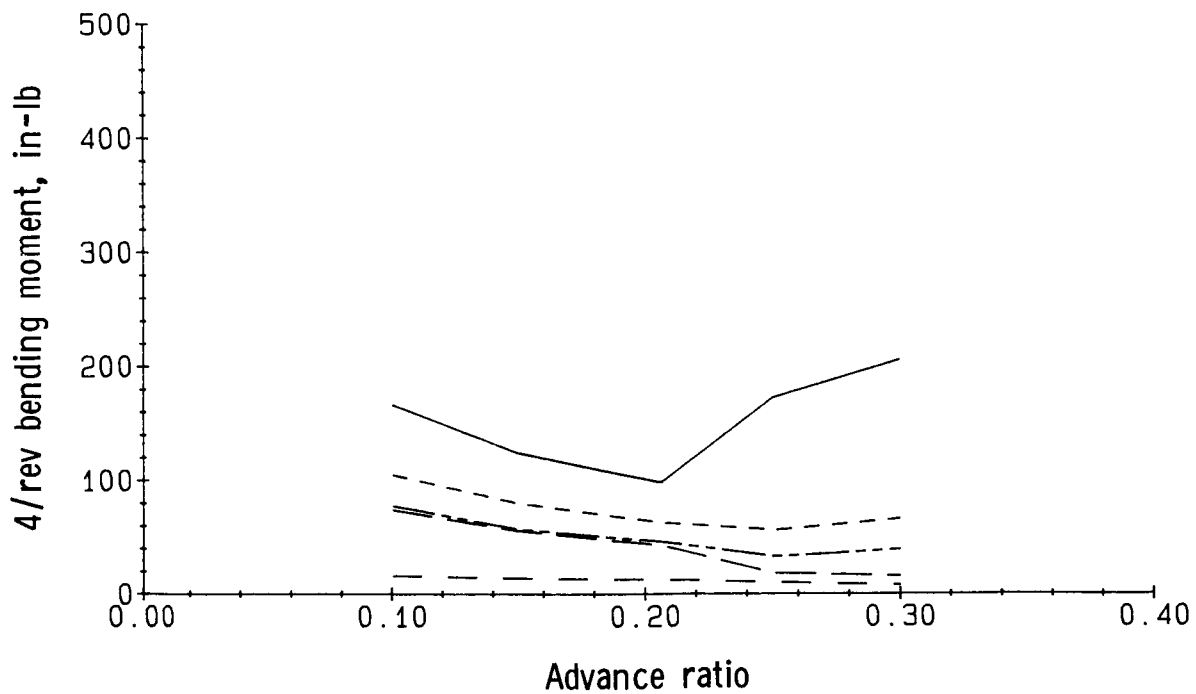
Figure 8.- Concluded.
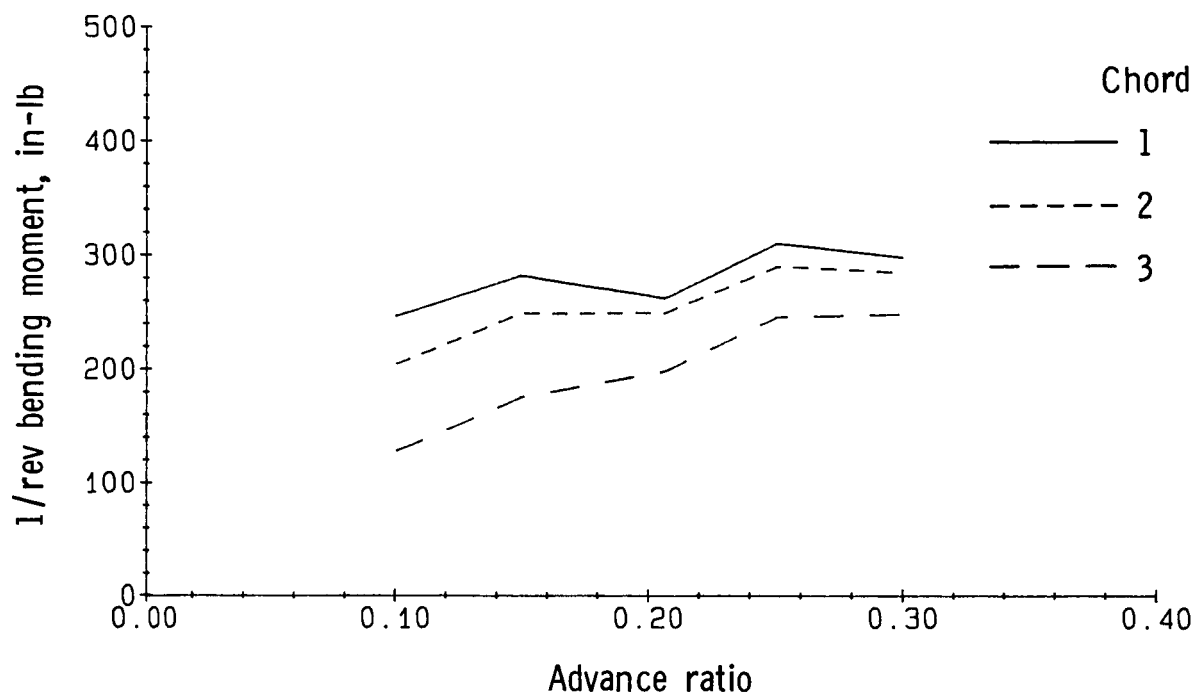
(a) 1/rev bending moment.
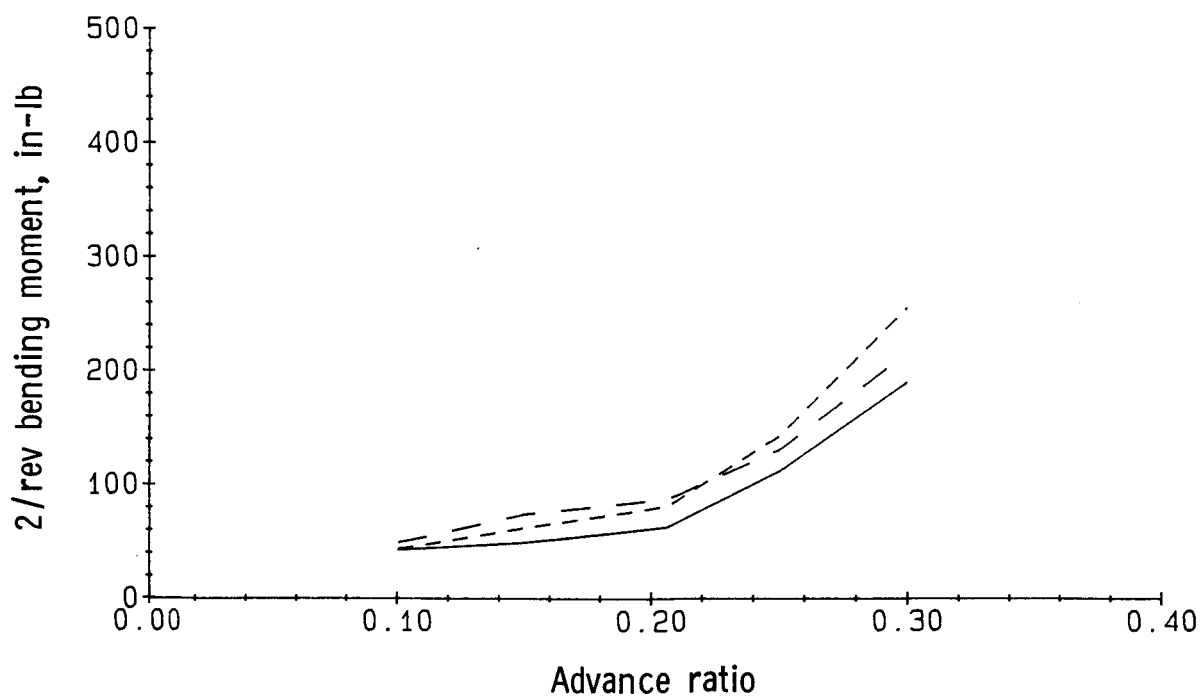
(b) 2/rev bending moment.

Figure 9.- Chord bending moment of advanced blade.
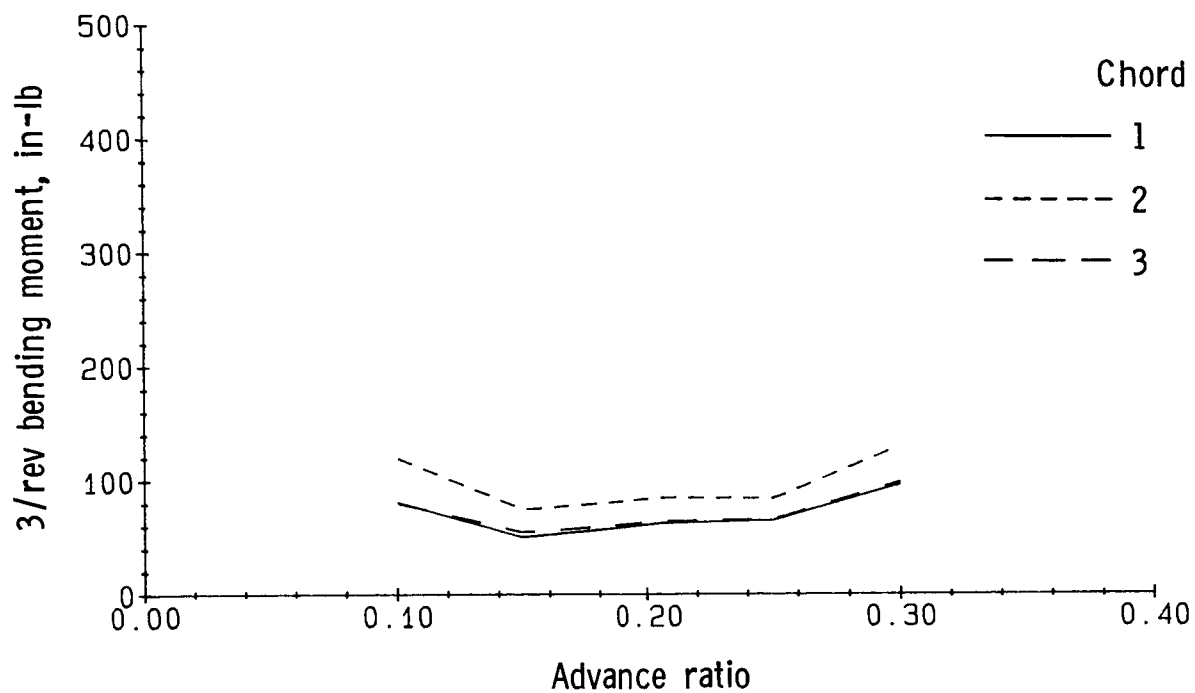
(c) 3/rev bending moment.

(d) 4/rev bending moment.

Figure 9.- Continued.

(e) 5/rev bending moment.

(f) 1/2 peak-to-peak bending moment.

Figure 9.- Concluded.

(a) 1/rev bending moment.

(b) 2/rev bending moment.

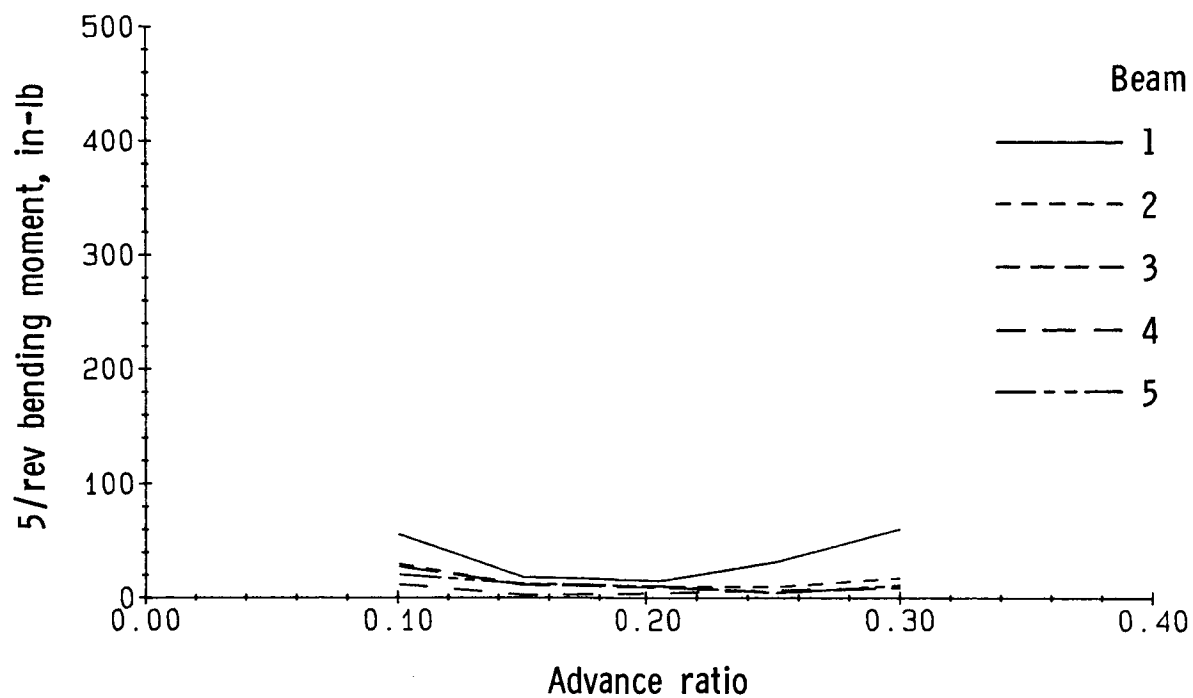Figure 10.- Beam bending moment of advanced blade.

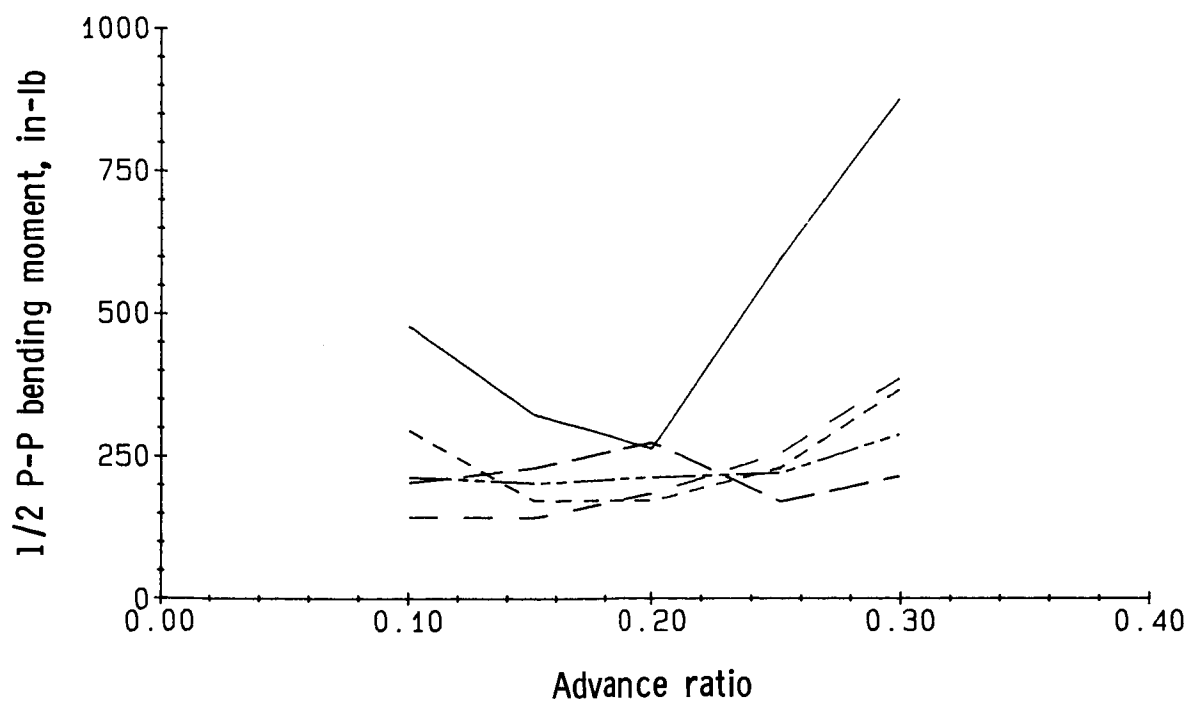(c) 3/rev bending moment.

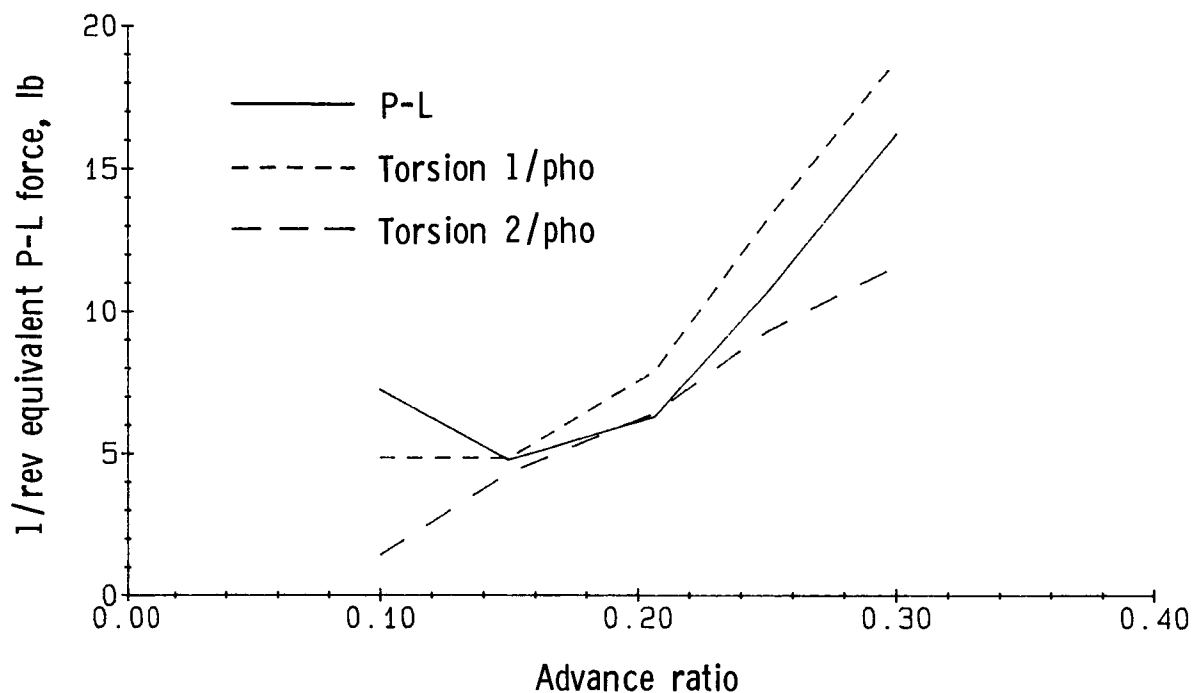(d) 4/rev bending moment.

Figure 10.- Continued.
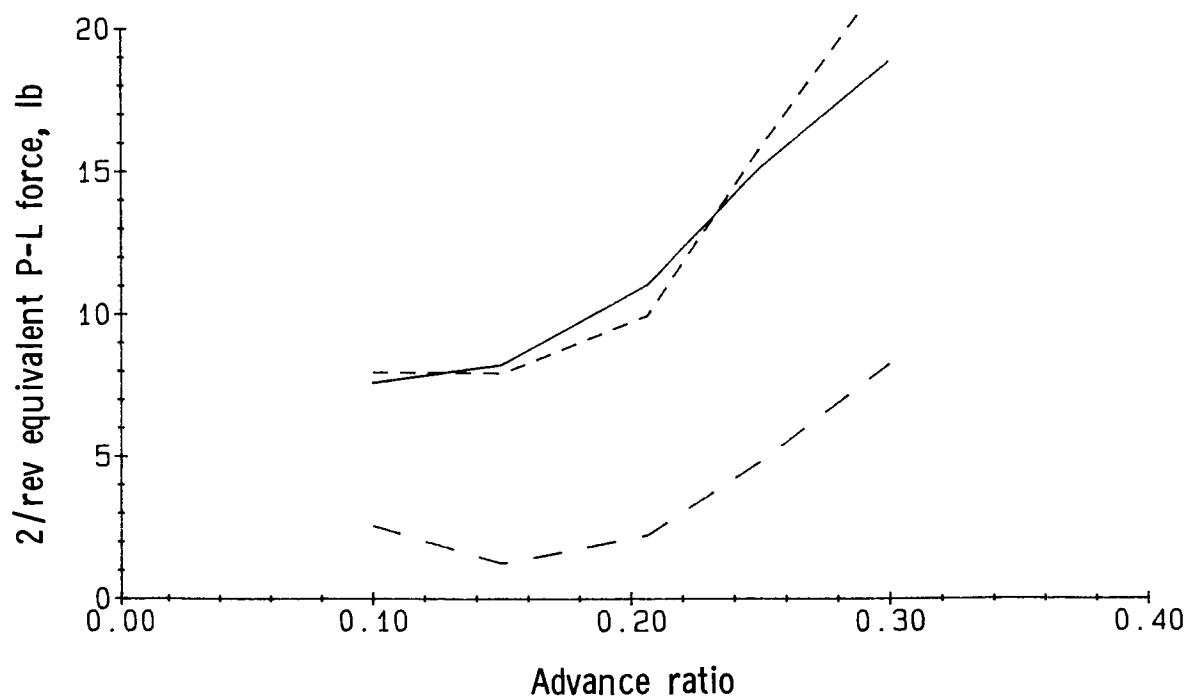
(e) 5/rev bending moment.

(f) 1/2 peak-to-peak bending moment.
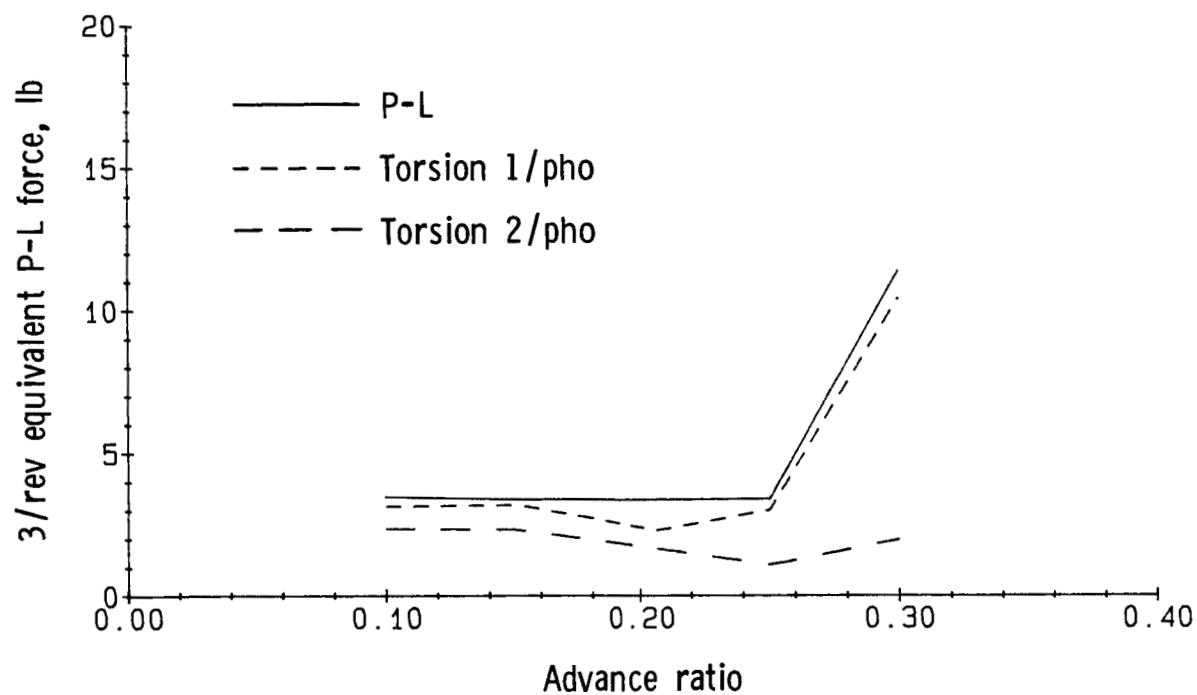
Figure 10.- Concluded.

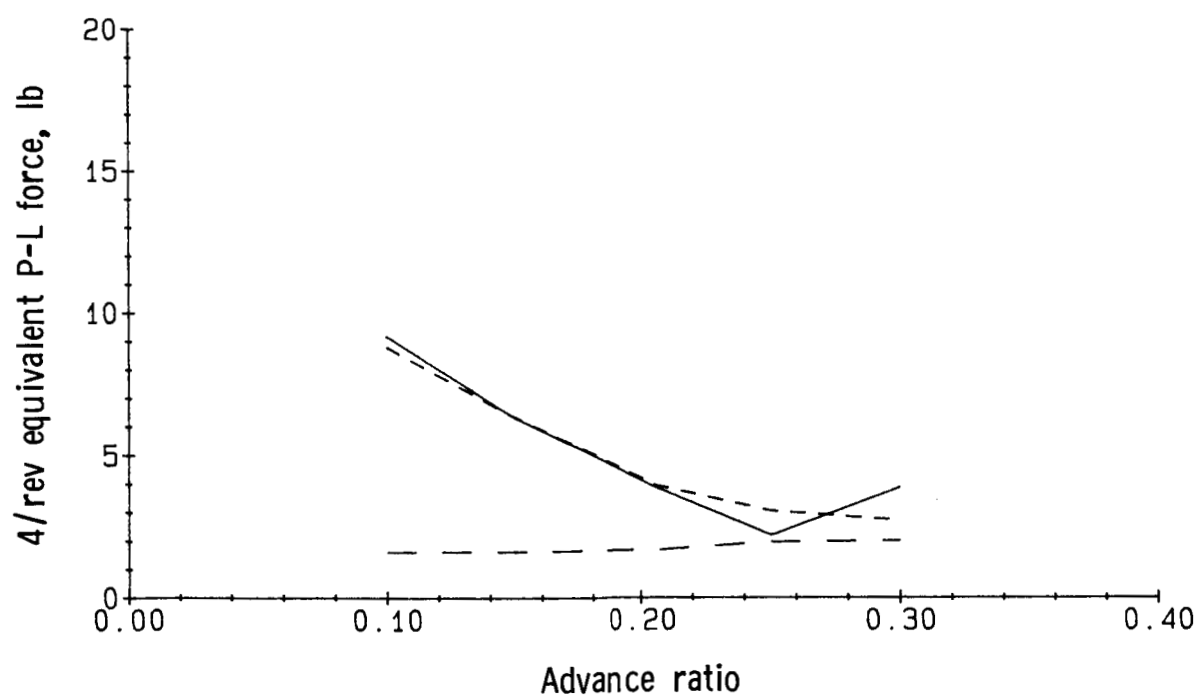(a) 1/rev equivalent pitch-link force.

(b) 2/rev equivalent pitch-link force.

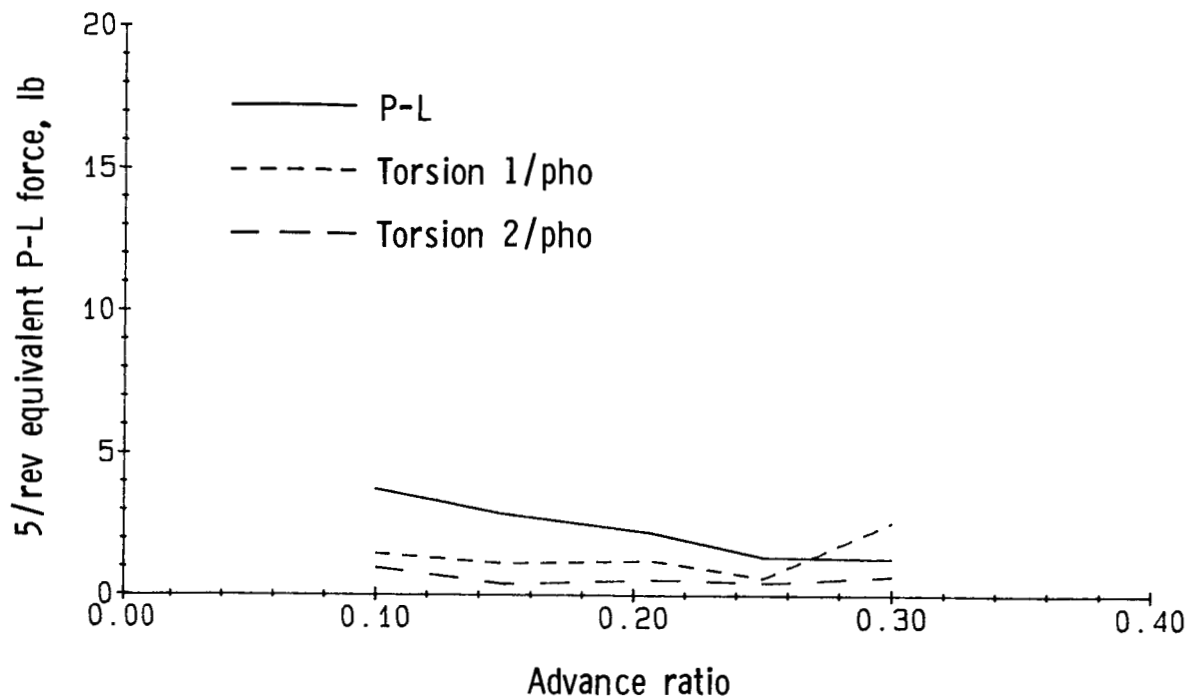Figure 11.- Equivalent pitch-link forces of advanced blade.
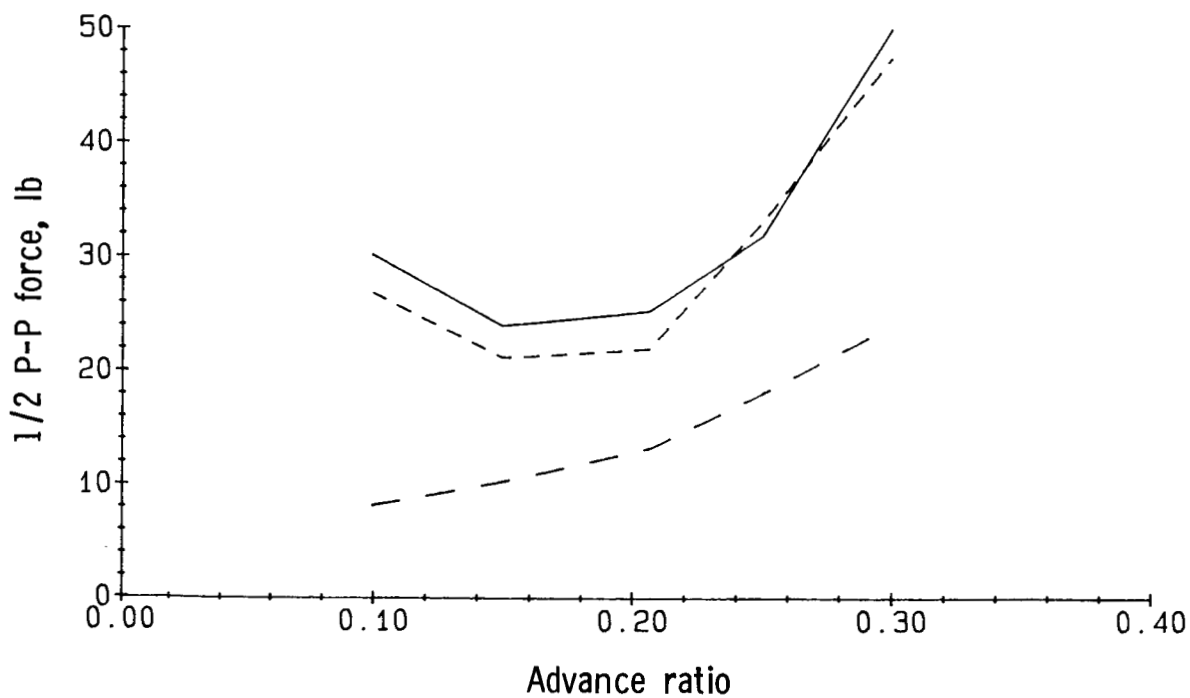
(c) 3/rev equivalent pitch-link force.

(d) 4/rev equivalent pitch-link force.

Figure 11.- Continued.

39

(e) 5/rev equivalent pitch-link force.

(f) 1/2 peak-to-peak force.

Figure 11.- Concluded.

APPENDIX

ANALYSIS OF STEADY LOADS

The data for the steady loads from the transducers on the blades have been analyzed more critically than the data for the oscillatory loads. The strain transducers were found to respond not only to bending in the principal axis intended but also to elongational strain due to centrifugal loading. A static test was conducted therefore to determine the sensitivity of the bending and torsion gauges to spanwise loading.

In normal operation, the spanwise load at a point on the blade is related to the centripetal accelerations on the total mass outboard of the specified point. To determine the effect of spanwise loading on the blade instrumentation, a uniform load was applied at the tip of the blade and was aligned with the blade quarter-chord axis. It was not possible to load the inboard sections to their full rotationally induced loads during the static test for two reasons: (1) the structure in the outboard stations was designed to withstand only the local axial loads due to rotational accelerations, and (2) it was difficult to grip the tip section safely for the loading process. The spanwise load was applied statically and was limited to 100 lb acting through all the gauge stations. Results of the axial load test are presented in figures A1 and A2. A straight-line least-squares curve fit was applied to the data to determine a sensitivity constant, which when multiplied by the local load results in a steady offset in gauge reading.

The assumption that loads induced by centripetal acceleration are static rather than dynamic is justified on the following basis. Small variations in actual rotational speed are highly damped by rotor inertia. Variations for radial distance due to cosine shortening in flapping and lead-lag motion are extremely small. The strain due to this centrifugal loading can therefore be considered a static effect. To predict the loads due to rotational acceleration, the mass distributions must be used. For both blades tested the mass distribution can be approximated by linear segments. By integrating from the outboard segments, the axial load due to centripetal acceleration can be computed for each of the gauge stations.

The loads predicted for the test rotational speed used in obtaining the data are presented in table AI. The radii, mass distributions, and rotational speed used are found in the basic report. Table AII shows the extrapolated values of static offset predicted by the axial load sensitivity and the predicted axial load.

Because the static loads applied were less than those induced through rotational acceleration, the gauge response to the rotational load must be extrapolated from the static load test. Because of the low static strain levels, confidence in this extrapolation is low and no mean loads data are reported.

TABLE AI.- AXIAL LOAD DISTRIBUTIONS

[Computed data]

Gauge	Baseline blade		Advanced blade	
	r/R	Axial load, lb	r/R	Axial load, lb
Chord 1	0.10	4108.2	0.18	2887.9
Chord 2	0.36	3758.9	0.28	2702.4
Chord 3	0.60	2925.4	0.47	2195.9
Beam 1	0.19	4108.2	0.18	2887.9
Beam 2	0.36	3758.9	0.28	2702.4
Beam 3	0.60	2925.4	0.47	2195.9
Beam 4	0.77	2082.4	0.60	1663.9
Beam 5	0.93	721.2	0.77	816.1
Torsion 1	0.36	3758.9	0.28	2702.4
Torsion 2	0.93	721.2	0.77	816.1

TABLE AII.- STATIC OFFSET DUE TO AXIAL LOAD

[Extrapolated data]

Gauge	Baseline blade		Advanced blade	
	r/R	Offset load, in-lb	r/R	Offset load, in-lb
Chord 1	0.19	-1192.1	0.18	-960.2
Chord 2	0.36	-934.5	0.28	129.9
Chord 3	0.60	-690.8	0.47	-333.9
Beam 1	0.19	113.9	0.18	64.1
Beam 2	0.36	(a)	0.28	-8.9
Beam 3	0.60	-207.7	0.47	-210.1
Beam 4	0.77	-204.5	0.60	-220.4
Beam 5	0.93	-89.4	0.77	-155.9
Torsion 1	0.36	-13.3	0.28	45.0
Torsion 2	0.93	-18.2	0.77	7.9

[a]Gauge malfunction.

(a) Chord bending-moment gauges.

(b) Beam bending-moment gauges.

(c) Torsion gauges.
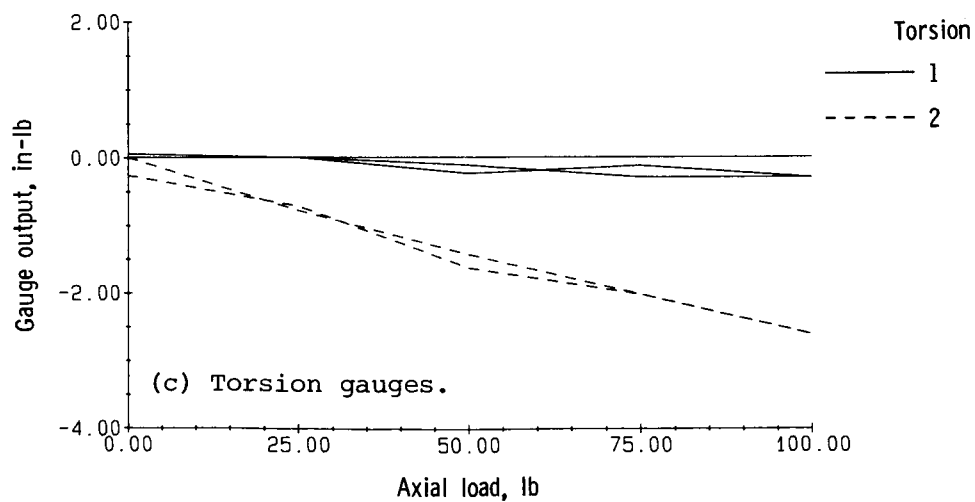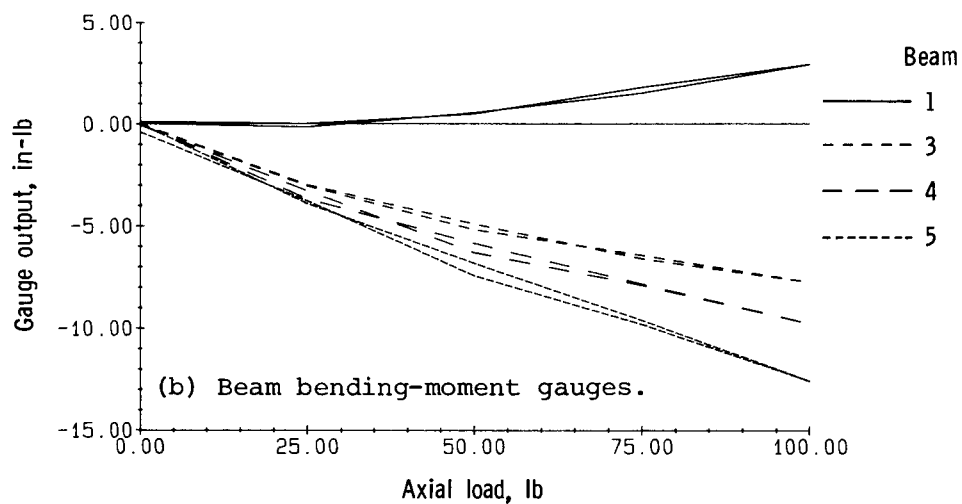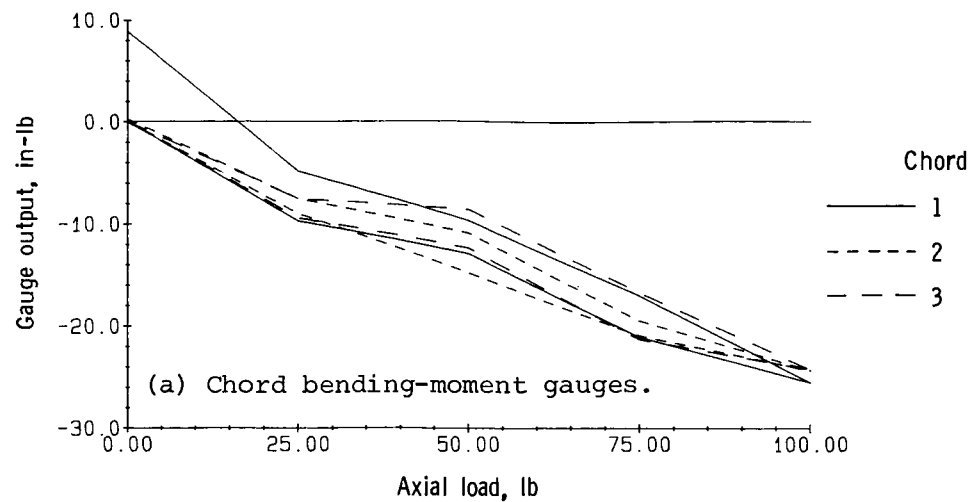
Figure A1.- Gauge sensitivity to axial load of baseline blade.

(a) Chord bending-moment gauges.

(b) Beam bending-moment gauges.
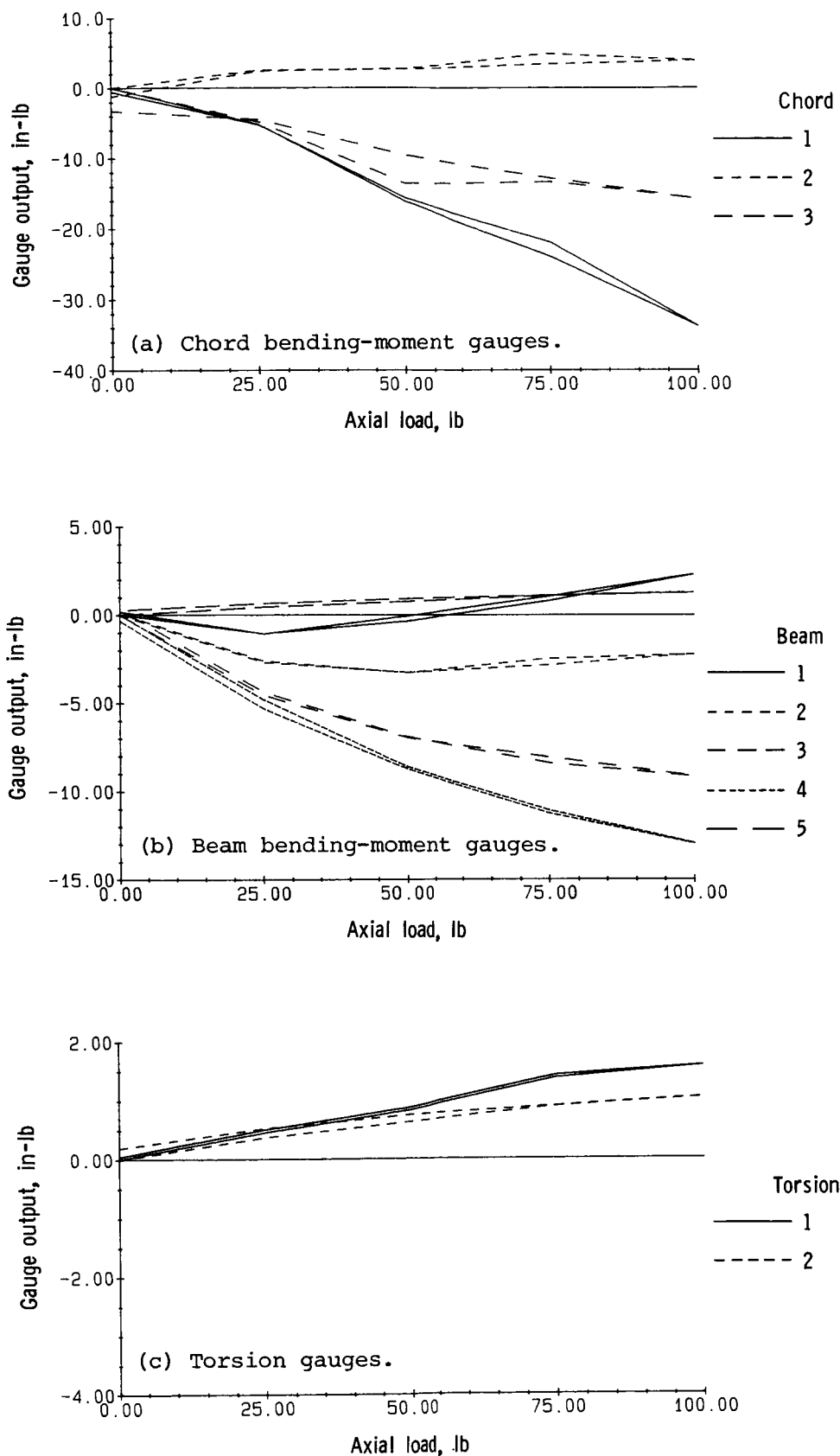
(c) Torsion gauges.

Figure A2.- Gauge sensitivity to axial load of advanced blade.

1. Report No. NASA TM-89053 AVSCOM TM 87-B-7	2. Government Accession No.	3. Recipient's Catalog No.
4. Title and Subtitle Helicopter Blade Dynamic Loads Measured During Performance Testing of Two Scaled Rotors		5. Report Date July 1987
		6. Performing Organization Code
7. Author(s) John D. Berry		8. Performing Organization Report No. L-16245
9. Performing Organization Name and Address Aerostructures Directorate USAARTA-AVSCOM Langley Research Center Hampton, VA 23665-5225		10. Work Unit No. 505-61-51-10
		11. Contract or Grant No.
12. Sponsoring Agency Name and Address National Aeronautics and Space Administration Washington, DC 20546-0001 and U.S. Army Aviation Systems Command St. Louis, MO 63120-1798		13. Type of Report and Period Covered Technical Memorandum
		14. Army Project No. 1L162209AH76

15. Supplementary Notes

John D. Berry: Aerostructures Directorate, USAARTA-AVSCOM.

16. Abstract

A test to determine the performance differences between the 27-percent-scale models of two rotors for the U.S. Army AH-64 helicopter was conducted in the Langley 14- by 22-Foot Subsonic Tunnel. One rotor, referred to as the "baseline rotor," simulated the geometry and dynamic characteristics of the production baseline rotor, and the other rotor, referred to as the "advanced rotor," was designed to have improved hover performance. During the performance test, the dynamic pitch-link forces and blade bending and torsion moments were also measured. Dynamic data from the forward flight investigation have been reduced and are presented herein. The advanced blade set was designed to have dynamic characteristics similar to those of the baseline rotor so that test conditions would not be limited by potential rotor instability and blade resonances and so that the measured performance increments could be considered to be due purely to aerodynamic causes. Data show consistent trends with advance ratio for both blade sets with generally higher oscillatory loads occurring for the advanced blade set when compared with the baseline blade set.

17. Key Words (Suggested by Author(s)) Helicopter Blade loads Dynamics Wind tunnel Scaled rotor	18. Distribution Statement Unclassified – Unlimited Subject Category 02		
19. Security Classif. (of this report) Unclassified	20. Security Classif. (of this page) Unclassified	21. No. of Pages 48	22. Price* A03